Effects of the tropospheric large-scale circulation on European winter temperatures during the period of amplified Arctic warming

Vihma, Timo; Graversen, Rune; Chen, Linling; Handorf, Dörthe; Skific, Natasa ...

2020-01

John Wiley and Sons Ltd

http://hdl.handle.net/10138/314241

Vihma, T, Graversen, R, Chen, L, Handorf, D, Skific, N, Francis, J A, Tyrrell, N, Hall, R, Hanna, E, Uotila, P, Dethloff, K, Karpechko, A, Björnsson, H & Overland, J E 2020, 'Effects of the tropospheric large-scale circulation on European winter temperatures during the period of amplified Arctic warming', International Journal of Climatology, vol. 40, no. 1, pp. 509-529. https://doi.org/10.1002/joc.6225

Effects of the tropospheric large-scale circulation on European winter temperatures during the period of amplified Arctic warming

Timo Vihma[1], Rune Graversen[2], Linling Chen[3], Dörthe Handorf[4], Natasa Skific[5], Jennifer A. Francis[6], Nicholas Tyrrell[1], Richard Hall[7], Edward Hanna[7], Petteri Uotila[8], Klaus Dethloff[4], Alexey Yu. Karpechko[1], Halldor Björnsson[9], James E. Overland[10]

[1] Finnish Meteorological Institute, Helsinki, Finland

[2] Department of Physics and Technology, University of Tromsø, Norway

[3] Nansen Environmental and Remote Sensing Centre, Bergen, Norway

[4] Alfred Wegener Institute, Helmholtz Center for Polar and Marine Research, Potsdam, Germany

[5] Department of Marine and Coastal Sciences, Rutgers University, USA

[6] Woods Hole Research Center, USA

[7] School of Geography and Lincoln Centre for Water and Planetary Health, University of Lincoln, UK

[8] Atmospheric and Earth System Research (INAR)/ Physics, University of Helsinki, Finland

[9] Icelandic Meteorological Office, Reykjavik, Iceland

[10] NOAA/Pacific Marine Environmental Laboratory, USA

Corresponding author:
Prof. Timo Vihma
Finnish Meteorological Institute
P.O. Box 503, Erik Palmenin aukio 1
00101 Helsinki, Finland
Email: timo.vihma@fmi.fi
Phone: +358 50 412 6365

Key words: Arctic, European weather, teleconnections, North Atlantic Oscillation, Scandinavian Pattern, subsidence heating

Abstract

We investigate factors influencing European winter (DJFM) air temperatures for the period 1979-2015 with the focus on changes during the recent period of rapid Arctic warming (1998-2015). We employ meteorological reanalyses analysed with a combination of correlation analysis, two pattern clustering techniques, and back-trajectory airmass identification. In all five selected European regions, severe cold winter events lasting at least four days are significantly correlated with ~~a~~ warm Arctic episodes. Relationships during opposite conditions of warm Europe/cold Arctic are also significant. Correlations have become consistently stronger since 1998. Large-scale pattern analysis reveals that cold spells are associated with the negative phase of the North Atlantic Oscillation (NAO-) and the positive phase of the Scandinavian (SCA+) pattern, which in turn are correlated with the divergence of dry static energy transport. Warm European extremes are associated with opposite phases of these patterns and the convergence of latent heat transport. Airmass trajectory analysis is consistent with these findings, as airmasses associated with extreme cold events typically originate over continents, while warm events tend to occur with prevailing maritime airmasses. Despite A~~a~~rctic-wide warming, significant cooling has occurred in northeastern Europe owing to a decrease in adiabatic subsidence heating in airmasses arriving from the southeast, along with increased occurrence of circulation patterns favouring low temperature advection. These dynamic effects dominated over the increased mean temperature of most circulation patterns. Lagged correlation analysis reveals that SCA- and NAO+ are typically preceded by cold Arctic anomalies during the previous 2 to 3 months, which may aid seasonal forecasting. 250 words (maximum is 250)

1. Introduction

Coincident with rapid warming in the Arctic, extreme weather events have become increasingly common in mid-latitudes (IPCC, 2012; Munich Re, 2018), with possible causal linkages between these

trends (Cohen et al., 2014; 2017; Coumou et al., 2014; Masato et al., 2014; Kug et al., 2015; Overland et al., 2016; Francis, 2017; Vihma, 2017; Vavrus, 2018). Arctic amplification (AA) has been suggested as contributing to an increased occurrence of persistent weather patterns (Masato et al., 2014; Hanna et al., 2016; Petoukhov et al., 2013; Kornhuber et al., 2017, Mann et al., 2017), and especially to winter cold spells in mid-latitudes, mainly in East Asia (Kug et al., 2015) and North America (Francis, 2017; Cohen et al, 2018; Overland and Wang, 2018) but also in the UK (Hanna et al., 2017). However, potential Arctic effects on continental Europe in winter have remained less clear (Overland et al., 2015), owing to other forcings from different locations, e.g., from the North Atlantic and tropics (Cassou et al., 2004; Buckley et al., 2016; Zappa and Shepherd, 2017), which makes it challenging to distinguish the impacts from the Arctic.

It is known that the negative phase of the North Atlantic Oscillation (NAO) is associated with anomalously cold and dry winters in most of Europe, whereas the positive phase of NAO is often associated with anomalously warm and moist winters (Marshall et al., 2001; Hurrell et al., 2003; Hanna and Cropper 2017). However, the NAO phase alone does not explain all aspects of the influence of atmospheric circulation over the North Atlantic on Europe (Vautard, 1990). The state of atmospheric circulation in the North Atlantic region also varies with episodes of Greenland Blocking (Hanna et al., 2016, 2018), the Scandinavian Pattern (Bueh and Nakamura, 2007), East Atlantic Pattern (Barnston and Livezey, 1987; Bojariu and Reverdin, 2002), and the East Atlantic / West Russia Pattern (Lim, 2015) that also influence European winter weather. Furthermore, Arctic and North Atlantic influences on Europe are likely connected. In addition to Greenland Blocking, this connection is seen in at least the following: (a) synoptic and large-scale circulation over the North Atlantic and Nordic seas strongly affects the occurrence and strength of Arctic cold-air outbreaks and polar lows reaching Europe (Kolstad et al., 2009), and (b) the AA impact on the NAO. Several recent studies suggest that warm Arctic episodes favour a negative NAO (Kim et al., 2014; Nakamura et al., 2015; Francis and Skific,

2015; Deser et al., 2016), but not consistently (Singarayer et al., 2006; Screen et al., 2014, Smith et al. 2017).

During 1956 to 2005, cold winters in Europe ~~were~~ seemed rarely linked with negative sea-ice anomalies in the Arctic (Yang and Christensen, 2012), but in recent years of dramatically reduced sea ice, there are indications that this ~~these~~ relationship has appeared and is ~~s are changing and~~ becoming increasingly~~more~~ robust. Grassi et al. (2013) notes that Barents-Kara sea-ice reduction favours a wintertime increase in the occurrence and intensity of extreme cold events over continental Europe along with extreme precipitation events over the Mediterranean basin. Observed reductions in autumn–winter Arctic sea ice, especially in the Barents and Kara seas, are correlated with strengthened anticyclonic circulation anomalies over the Arctic Ocean, which tend to induce easterly flow and cold-air advection over northern Europe (Cohen et al., 2014). Model simulations suggest that sea-ice decline in the Canadian Archipelago and Baffin Bay links with cold-air outbreaks over central Europe during October – March (Screen, 2017). In these months, sea-ice loss in the Barents–Kara Seas results in drying over northwest Europe and a decrease in 500 hPa geopotential heights extending from the mid-Atlantic to eastern Europe at roughly 40°N, resembling a negative phase of the NAO. According to Koenigk et al. (2016), winter temperatures in central and western Europe are most strongly correlated with Greenland Sea ice variability.

The most direct effect of AA on mid-latitude winter weather is that cold-air outbreaks originating from the Arctic are not as cold as they were in the 1980s and 1990s (Serreze et al., 2011; Screen, 2014), except in East Asia (Kim et al., 2014). However, the Arctic's influence is often transmitted via more complex mechanisms, including changes in (a) latitude, speed, and meandering of the polar front jet stream (Vavrus et al., 2017; Zappa et al., 2018), (b) blocking occurrence, strength, and location (Masato et al., 2014; Hanna et al., 2016; 2018), and (c) wintertime stratosphere-

troposphere coupling (Handorf et al., 2015; Crasemann et al., 2017; Kretchmer et al., 2016; Hoshi et al., 2019).

This study addresses the question: How does the tropospheric large-scale circulation affect European air temperatures in winter (defined as DJFM), and have these effects changed during the period of AA? We address years 1979-2015, focusing on differences between the first and second half of the period, the latter corresponding to the start of the rapid AA (Vavrus et al., 2017; Davy et al., 2018; Overland et al., 2019). The study is based on atmospheric reanalysis products that are analysed by applying multiple approaches and methods to address the occurrence of daily air temperature extremes in Europe and the Arctic, large-scale circulation patterns affecting European weather, and origin of airmasses advected to Europe.

2. Methods

2.1 Analyses of air temperature anomalies

Five study regions of Europe were chosen~~identified~~: CE: Central Europe 45°N-55°N, 0°-20°E; SE: Southern Europe 35°N-45°N, 10°W-35°E; NE: Northern Europe 55°N-70°N, 5°E-25°E; WE: Western Europe 50°N-60°N, 10°W-5°E; EE: Eastern Europe 45°N-55°N, 20°E-40°E (**Figure 1**). Data for 2-m air temperatures (T2m) were obtained from the ERA-Interim reanalysis (Dee et al., 2011) for 1979 to 2015. For each region the mean area-weighted T2m for the region was calculated for each day, and then converted to standardised anomalies relative to 1981-2010 climatology for each day, removing the seasonal cycle. Significant temperature anomaly events in each region were defined as the detrended temperature anomaly being greater than or equal to +1.75 standard deviation (SD) for at least four consecutive days for the positive anomalies (hereafter called as warm events), and less than or equal to -2 SD for at least four consecutive days for the negative anomalies (hereafter called as cold events).

The different thresholds for positive and negative anomalies were applied to ensure samples of similar size.

Trends in the number of days when warm/cold events occurred were assessed for significance (95% confidence) using the Mann-Kendall trend test, with consideration of autocorrelation in the time series (Yue and Wang, 2004). In order to demonstrate the possible relation of these events with AA, we created composite maps of Northern Hemisphere T2m related to the cold/warm events in these five regions.

Central Arctic warm events are defined as periods of four or more consecutive days when the detrended T2m anomaly, averaged over 80-90°N, is greater than 1.75 SD above the 1981-2010 climatology.. Greenland Blocking episodes are identified as four or more consecutive days when the Greenland Blocking Index (GBI) is more than 2 SD above 1981-2010 climatology (Hanna et al., 2018). The GBI is defined using the mean 500 hPa geopotential height for the 60-80^{o}N, 20-80^{o}W region (Hanna et al., 2016).

2.2 Analyses of large-scale circulation

Self-Organizing Maps (SOM; Kohonen 2001) were applied to classify daily ERA-Interim 500 hPa geopotential height anomaly fields throughout 1979-2015. The SOM algorithm is initialized using the first two EOFs of the data vectors to ultimately create a matrix of representative spatial patterns, with the matrix size defined by the user. In the SOM training, individual geopotential height anomaly fields are presented to the SOM and a Euclidean measure of distance is compared between the anomaly field and each pattern to determine the "winning" pattern, which has the smallest Euclidean distance to the anomaly field. As each new field is presented, the winning pattern and neighbouring patterns are updated iteratively reducing the difference against the anomaly field (Hewitson and Crane 2002). In this way the SOM algorithm organizes the patterns (also called nodes) so that similar daily fields are

clustered into one pattern, and the patterns are presented such that those most different from each other are in the opposite corners of a two-dimensional array of 'self-organized' patterns as shown in **Figure 2**. The SOM algorithm objectively classifies atmospheric circulation anomalies; this approach objectively identifies weather patterns that affect European temperatures.

We selected a matrix size of 12 as a suitable number of nodes as a balance between identifying distinct patterns and providing sufficient detail. We then identified the most frequently occurring patterns and named them according to the well-known large-scale circulation patterns that they resemble. The SOM algorithm keeps track of which daily fields belong in each of the 12 patterns. This allowed us to project other variables of interest (such as anomalies of T2m and divergence of the dry-static energy and latent heat) onto the 12 circulation patterns. We also calculated the frequency of occurrence of each pattern, as well as frequency changes from 1979-1997 to 1998-2015.

The vertically integrated latent heat transport in the zonal and meridional directions is given by:

$$u E_Q = \int_0^{P_s} u L q \frac{dp}{g} \tag{1}$$

and

$$v E_Q = \int_0^{P_s} v L q \frac{dp}{g}, \tag{2}$$

where E_Q is the latent heat, u and v are zonal and meridional wind components, L is specific heat of condensation, q is air specific humidity, g is acceleration due to gravity, and p is pressure (subscript s referring to Earth surface). Transports were computed using variables at all ERA-Interim model hybrid

levels, a 6-hourly time resolution, and interpolated to 0.5 x 0.5 degree horizontal gridresolution. Due to a mass-flux inconsistency in reanalysis data (Trenberth, 1991), a barotropic mass-flux correction was applied to the wind field at each time step before the energy transport was calculated (Graversen, 2006). After computing the transports, the divergence of the vertically integrated transport and its anomaly was calculated. Analogous calculations yielded the anomaly of the divergence of vertically integrated transport of dry-static energy (in the equations, L q was replaced by $c_pT + g z$, where c_p is the specific heat capacity at constant pressure, T is air temperature, and z is height). Spatial correlation coefficients were calculated to quantify the relationship between the time-averaged fields of transport divergences and T2m anomalies.

To understand how the large-scale circulation patterns – as represented by the SOM nodes – that affect European weather arewere associated with Arctic temperatures, the T2m anomalies averaged over the circumpolar Arctic north of 70°N were calculated 90 days before and after the occurrence of the six most common SOM nodes (nodes 1, 3, 4, 9, 10, and 12).

As the results may be sensitive to the analysis methods and metrics, we also applied a different cluster analysis method (k-means cluster) to the same ERA-Interim fields to identify the most common 500 hPa circulation patterns over Europe and their changes. The cluster analysis was carried out over the North-Atlantic-Eurasian region (30° – 90°N, 90°W-90° E) for winter. The daily 500hPa geopotential height anomaly fields from ERA-Interim for the period 1979-2014 were analysed. We applied the same methodology as in Crasemann et al. (2017), which involves the reduction of the dimensionality of the data set by an Empirical Orthogonal Function (EOF) analysis and a subsequent k-means cluster analysis in the reduced state space spanned by the first 5 EOFs. As with SOM and other cluster algorithms, it is necessary to prescribe the number of clusters k as an input parameter. Here, we realize the identification of the most common 500 hPa circulation patterns by searching for non-Gaussian structures in the reduced state space (Cassou et al., 2004; Dawson and Palmer, 2015). By

performing Monte Carlo simulations, we tested the null hypothesis of the non-existence of non-Gaussian structures, i.e. multi-normal distribution of the probability density function, with the same approach as in Straus et al. (2007), and Dawson and Palmer (2015). Significance of the clustering has been estimated for k =2 - 8… clusters. k = 5 is the smallest significant partition size which is significant at the 95% level, therefore it is used as cluster size. By calculating histograms separately for periods 1979-1997 and 1998-2015, we detected changes in the relative frequency of occurrence of each circulation pattern in each of the winter months. The significance of the changes in each month was tested using a bootstrap test with 1000 bootstrap replicates for each regime and each month.

2.3 Analyses of airmass origin

To address the relationship of temperature anomalies with airmass transport into Europe, five-day backward trajectories were calculated for each day in 1979-2015 ending over ten selected European cities: Archangelsk, Berlin, Bucharest, Glasgow, Hammerfest, Helsinki, Kazan, Minsk, Moscow, and Rome. These cities were selected with an emphasis on northeastern Europe. The trajectories were calculated by applying the Meteorological Data Explorer (METEX) calculation service (Zeng et al., 2010), which utilizes the NCEP-CFSR reanalysis (Saha et al., 2010) with a spatial resolution of 0.5 x 0.5 degree. The METEX output includes hourly values along the trajectory of latitude, longitude, horizontal and vertical wind components, air temperature, atmospheric pressure, and the height above ground level. Accordingly, for each city and each day, we determined whether~~if~~ the trajectory start point (airmass origin) was in the Arctic (north of 70°N) and if it was located to the northeast, southeast, southwest, or northwest of the city in question. To avoid trajectories within the atmospheric boundary layer, where reanalyses are more prone to errors, the trajectories were set to end at the height of 1000 m above each city in question~~selected~~. The height difference between the trajectory start and end points allowed calculation of adiabatic subsidence heating (on the basis of dry-

adiabatic lapse rate of 0.0098 $^{o}C\ m^{-1}$, e.g., Stull (2001)) during the 5-day airflow along the trajectory. The distributions of airmass origin and related temperature changes between 1979-1997 and 1998-2015 were analysed utilizing results of the large-scale circulation patterns identified by the cluster analyses.

3. Results

3.1 Air temperature anomalies over Europe and the Arctic

Our analyses demonstrate that cold winter events, at least four days long, in all five European regions are significantly related to positive temperature anomalies in the Arctic. In WE, CE and NE, cold winter events are strongly associated with positive T2m anomalies over the Greenland/Baffin region. In SE and EE, however, cold winter events are associated with warm episodes in both the Greenland region and the Barents-Kara seas area (**Figure 3**, left column). The wintertime association of cold events in Europe and warm events in the central Arctic has become stronger: only a single combined occurrence meeting the threshold and duration criteria (Section 2.1) was observed during 1979-1997 but 6 to 10 events (depending if the trend is removed or not) during 1998-2015 (**Table 1**). The association with Greenland Blocking events has also become stronger (**Table 1**), which is not due to increase of cold events but due to increase in simultaneous occurrence of GBI events and European cold events. The opposite is also true. Warm winter events in all five European regions are associated with cold anomalies in the Arctic, but with remarkable regional differences (**Figure 3**, right column). Warm events in WE, CE, EE, and NE are associated with cold anomalies in Greenland and, in the case of NE, also in Alaska. However, warm events in SE are associated with cold anomalies in NE, the Nordic Seas, and central and northwestern North America, as well as with warm anomalies in the Labrador – Baffin region.

Relaxing the 4-day criteria, i.e., addressing individual days, there are significant positive correlations between the number of cold days per winter in Europe and the number of warm days per winter in Greenland and Barents-Kara seas (**Table 2**). This demonstrates that in terms of interannual variability between winters, cold conditions in WE, NE, and CE are associated with warm conditions in the Greenland region, while cold in EE and SE are associated with a warm Barents-Kara seas area. In contrast, all correlations between the number of warm days per winter in the five European regions and the number of cold days per winter in Greenland and Barents-Kara seas area are insignificant and mostly very close to zero (not shown). These results demonstrate a simultaneous correspondence between cold anomalies in the Arctic and warm events in the five European regions (**Figure 3**, right column), but that the Europe-Arctic relationship is weak in terms of interannual variations in the number of warm winter days in Europe and cold winter days in the Arctic.

Changes in these relationships over time are observed by comparing correlations between 1979-1997 and 1998-2015 (**Table 2**). Statistical relationships between the number of cold days in CE and NE and warm days in Greenland have become consistently stronger during the AA era, as have relationships between cold days in SE and EE and warm days in the Barents-Kara seas region.

3.2 Large-scale circulation patterns controlling European weather

3.2.1. Results based on SOM analyses

The most frequently occurring SOM patterns in descending order are 12, 3, 1, 4, 9, and 10 (**Figure 2**). Some of the nodes closely resemble patterns that are recognized as important for European weather: the NAO in its positive phase (nodes 3 and 4, hereafter called NAO+ nodes) and negative phase (9 and 10, NAO- nodes, also associated with the Greenland/Baffin--Bay blocking), as well as the Scandinavian Pattern in its positive (8, 11 and 12; SCA+) and negative phase (1, 2, and 5; SCA-). To understand the mechanisms responsible for the association of these circulation patterns with European winter

temperatures, we compare the transport divergence anomalies of latent heat (**Figure 4)** and dry static energy **(Figure 5)** projected on the SOM nodes against T2m anomalies (**Figure 6**). For clarity, only the six most common nodes are shown in **Figures 4, 5** and **6**.

The results demonstrate that over northern Europe the NAO+ nodes exhibit anomalous convergence of latent heat transport (i.e., negative anomaly in divergence, favouring positive temperature anomalies), whereas the NAO-/Greenland blocking nodes indicate anomalous divergence (favouring negative temperature anomalies). Considering dry static energy transport, the main differences from these associations are found in southern Europe, where NAO- is associated with anomalous divergence, and in Norway and Iceland, where NAO+ is associated with anomalous divergence. The SCA+ node shows anomalous divergence of latent heat transport over most of Europe, particularly in Scandinavia, whereas the SCA- node is associated with anomalous convergence mostly over Eastern Europe. In contrast, in the case of dry static energy transport, SCA+ is associated with anomalous convergence in northern Europe, particularly in Scandinavia, and SCA- is associated with anomalous divergence in most of Europe. A quantitative comparison of the resemblance between T2m anomaly patterns and those of the divergence of dry static energy and latent heat transports is presented in **Table 3.** The spatial correlation between the time-averaged T2m anomaly and the type of transport divergences over Europe (35-70ºN, 10ºW-60ºE) depends on the prevailing large-scale circulation. Averaged over cases of NAO- and SCA+, positive T2m anomalies are collocated with convergence of dry static energy transport as indicated by high spatial correlation coefficients, but they are weakly or not collocated with convergence of the latent heat transport. In contrast, in conditions of SCA- and NAO+, positive T2m anomalies are better collocated with convergence of latent heat than dry static energy transport (**Table 3**). However note that for all nodtes shown here, 2mT is showing high correlation to the total transport, and except for node 3, the correlations are higher than for the

individual components emphasizing the strong linkage between total atmospheric energy transport and local temperature anomalies.

The T2m anomalies related to the most common SOM nodes (**Figure 6**) are associated with patterns of cold and warm events in various parts of Europe. Cold events in CE and EE (**Figure 3**) can occur under all 12 SOM nodes, but are most common under SCA- (node 1;) (**Supplementary Table S1**). This is in accordance with large divergence of dry static energy under SCA- all over WE and CE (**Figure 5**), which dominates over small convergence of latent heat present in parts of WE and CE (**Figure 4**). Cold events in NE are most commonly associated with SOM nodes 1 and 12 (**Supplementary Table S1**). This result is interesting, as nodes 1 and 12 correspond to the opposite phases of SCA. However, transport divergence dominates under both phases: latent heat transport mostly diverges over NE for both SCA- and SCA+ (Figure 4), while dry static energy transport diverges for SCA- but converges for SCA+ (**Figure 5**). Warm events in WE and NE are in more than 65-69% of cases associated with SCA+ or NAO+ (node 3, 4, and 12; **Supplementary Table S1**). Convergence dominates in this region since for , as SCA+, favours divergence of latent heat transport is more than compensated for by along with convergence of dry static energy transport, and whereas NAO+ favours strong convergence for latent heat transport, with insignificant signals for dry static energy. Warm events in SE are more evenly distributed between different SOM nodes, and in EE there has been only a single four-day-long warm event meeting the 1.75 STD threshold, associated with NAO+, which is strongly associated with convergence of both latent heat and dry static energy transport.

The NAO+, NAO-, SCA+, and SCA+ nodes are closely associated with both European and Arctic temperature anomalies (**Figure 6**). A statistically significant relationship occurs between SCA- (node 1) and a cold central Arctic (north of 70°N), covering the period from 75 days before to 7 days after the occurrence of SCA- (**Figure 7**). Analogously, the central Arctic exhibits significant warm

anomalies in the period from 4 days before to 6 days after the occurrence of SCA+. However, NAO+ (nodes 3 and 4) is the pattern with the longest and most robust relationship with preceding Arctic winter temperature anomaly: about 90 days of statistically significant cold anomalies in the Arctic precede NAO+ node 3, and the relationship is almost as strong for NAO+ node 4. The occurrence of NAO- (nodes 9 and 10) is typically preceded by warm anomalies in the Arctic, but followed by anomalies that vary in sign with a period of approximately a month. This period is typical also for the variability of anomalies related SOM nodes 1, 4, and 12 (**Figure 7**).

Comparing winter periods in 1998-2015 and 1979-1997, the SOM nodes show, on average, more warming than cooling, but strong signals for cooling are present for nodes 3 (NAO+) and 12 (SCA+) in northeastern Europe and for node 9 (NAO-) in scattered locations (**Figure 8**). Furthermore, the occurrence of some circulation patterns has changed markedly (**Figure 9**). Those with high (low) height anomalies in high latitudes are predominantly more (less) frequent in recent winters. Occurrences have decreased for NAO+ ($p < 0.05$) and SCA- (insignificantly), while they have increased for NAO- ($p < 0.05$) and SCA+ (insignificantly). The results are similar for long-duration events (LDEs, lasting four or more days; **Figure 9**).

3.2.2 Results based on cluster analysis

The cluster analysis revealed five preferred circulation patterns (**Figure 10**), ordered according to their frequency of occurrence, which resemble (1) NAO+ (similar to SOM patterns 3 and 4), (2) the East-Atlantic/West-Russia pattern (EAWR+) that features high geopotential heights over the North Atlantic and Europe surrounded by negative anomalies, (3) SCA+ (resembling SOM pattern 12), (4) NAO- (resembling SOM patterns 9 and 10), and (5) a strong dipole structure in the east-west direction and positive height anomalies over the Atlantic and Greenland along with negative anomalies over Europe and the Barents Kara Sea (DIPOL, partly resembling SOM patterns 1 and 5). Comparing

periods 1998-2015 and 1979-1997, there are statistically significant increases in the frequency of occurrence of SCA+ in December and January and in the frequency of occurrence of NAO- in March (and in February at 90% significance level). In addition, blocking over the North Atlantic (DIPOL, in February) and in late winter over the British Isles / North Sea (EAWR+, in March) occurred significantly more frequently during 1998-2015. Accordingly, the results in **Figure 10** support conclusions based on the SOM analysis in **Figure 9**.

Next we compare T2-m anomalies for each SOM node (**Figure 6**) and for each pattern revealed by the cluster analysis (**Supplementary Figure S1**). Considering NAO-, T2m anomalies based on the SOM and cluster methods are qualitatively similar, but in Central Europe the cluster analysis reveals anomalies that are not as cold as those in the SOM analysis. Also, the positive anomalies in the Greenland-Baffin region are located farther west in the cluster results. Both negative and positive T2m anomalies related to NAO+ are somewhat stronger in the SOM-based results, but in the Barents and Greenland seas the differences between the two SOM nodes associated with NAO+ (nodes 3 and 4) are larger than the differences between SOM- and cluster-based results. For SCA+, SOM analysis yields stronger T2m anomalies in Central Europe and Greenland. The SOM-Cluster analysis differences reported above are due to the differences in the population of Z500 fields belonging to certain SOM nodes and clusters (compare **Figures 2** and **10**). The more extreme negative and positive T2m anomalies based on SOM analysis are due to the six most common SOM nodes representing 66% of the daily data from 1979-2015, whereas the five clusters together cover all the data. The cluster analysis reveals the EAWR and DIPOL patterns and the associated T2m anomaly fields, such as the European warm anomalies solely in Scandinavia and Iceland under EAWR and solely in Russia under DIPOL, which are not present in the SOM-based results. Hence, application of the two analysis methods is complementary, and reveals information on the sensitivity of the results to the method applied, and perhaps the differing spatial domains of the analyses.

Considering T2m changes between 1979-1997 and 1998-2015, results based on SOM (**Figure 8**) and cluster (**Supplementary Figure S2**) analyses are qualitatively similar, but include the following differences. For the patterns that resemble NAO+, the cluster analysis shows warming almost everywhere, but the SOM analysis also reveals regions of cooling, e.g., to the east and northeast of the Caspian Sea. For NAO- the largest differences occur in Greenland, with cooling based on SOM analyses and warming based on cluster analyses. For SCA+ the European cooling is shifted farther northeast in the cluster-based results.

3.3. Airmass transport to Europe

Changes in the occurrence of large-scale circulation patterns and the air temperatures associated with each pattern are expected to be reflected in the temperatures of airmasses of different origin transported to Europe, which motivated us to analyse airmass trajectories.

Among the ten selected cities (Section 2.3), the daily occurrence of air masses with Arctic (here defined as north of 70°N) origin varied from 4% in Rome to 40% in Hammerfest. Comparing the period 1998-2015 against 1979-1997, in all ten cities the occurrence of Arctic-origin airmasses has remained essentially the same, and the temperatures of Arctic-origin air have increased on average by 0.5°C. This equals the temperature increase averaged over all airmass origins for the ten cities. However, the warming under Arctic-origin air has not been uniform throughout the winter. In all cities with considerable occurrence (> x %) of Arctic airmasses, the temperatures have increased in December and January but decreased in March. The early-winter warming has been strongest in Hammerfest and Minsk (1.8°C) and the March cooling has been strongest in Helsinki and Archangelsk (-1.5°C). Airmasses of Arctic origin occur under all five circulation patterns based on the cluster

analyses, but they are most common in the NAO- pattern (24% of cases) and least common in the SCA+ pattern (11%).

We next focus on the direction instead of the latitude of airmass origin. In cases of airmasses coming from the northeast, northwest or southwest, the period 1998-2015 has been warmer than the period 1979-1997 in all ten cities (**Figure 11**). However, in cases of southeasterly airmass origin, cooling occurred in the eastern-most cities of Kazan (-1.0°C), Moscow (-0.8°C), Helsinki (-0.7°C), and Archangelsk (-0.5°C). If the general warming trend (averaged over all airmass origins) is removed from the time series, the cooling is significant ($p < 0.01$) in Kazan, Helsinki and Moscow.

The winter cooling in cases of southeasterly airmass origin was associated with changes in the occurrence of different large-scale circulation patterns (**Table 4**) and with the mean temperature and its change under each pattern (**Figure 12**). We identify the change in a pattern occurrence as the dynamic effect, and the change in the mean temperature of a pattern as the thermodynamic effect. The dynamical factors associated with a southeasterly airmass origin are as follows. In the four eastern-most cities (Archangelsk, Helsinki, Kazan and Moscow), NAO- is associated with the lowest or second-lowest (in Kazan) air temperature (**Figure 12a**), and the NAO- pattern has become increasingly common (**Table 4**). In contrast, the occurrence of NAO+, which is the warmest or second-warmest (in Archangelsk) pattern, has strongly decreased. Further, in Archangelsk the cooling is also related to the ~~decreased occurrence of SCA+, which is the warmest pattern there, and to the~~ slightly increased occurrence of the rather cold DIPOL pattern. Thermodynamic factors also contributed to the cooling: cooling of the DIPOL pattern in Archangelsk and cooling of the SCA+ pattern in Kazan (see also **Figure 8**). The following factors opposed the cooling but did not dominate over it: thermodynamic warming of the NAO+ and NAO- patterns in all four cities, and an increased occurrence (dynamic factor) of the warm SCA+ pattern in Kazan (**Figure 12, Table 4)**.

As in the case of temperature changes for Arctic airmass origin, the cooling in cases of southeasterly airmass origin has not been uniform throughout the winter. The winter averages are dominated by cooling during March in Kazan, Archangelsk, and Moscow, with monthly mean values of -1.8, -1.3, and -0.8 K, respectively. As was the case for the entire winter, we find that during March the principal dynamic effect responsible for cooling in all three cities, is the significantly increased occurrence of NAO- (**Supplementary Table S2**). The other dynamic effects are as follows. In Kazan in March, the DIPOL pattern is warm, and its occurrence has strongly decreased. In Archangelsk, SCA+ and NAO+ are the warmest patterns, and their occurrences have decreased. In Moscow, NAO+ is the warmest pattern with a decreased occurrence.

Common changes in Archangelsk, Helsinki, Kazan and Moscow were (i) a decrease of subsidence along the airmass trajectories (**Supplementary Figure S3.**) and, as a minor effect, (ii) low-tropospheric cooling at the trajectory starting points. Averaged over the four cities, the mean height of the starting points of the trajectories was 1750 m in 1979-1997 but only 1480 m in 1998-2015. Hence, as the calculations were set so that all trajectories ended at the same height (1000 m), during 1998-2015 there was on average 2.6°C less adiabatic subsidence heating during the 5-day airflow. This alone would have caused an even larger temperature decrease than observed in the four cities (**Figure 11**), but diabatic heating/cooling processes were also active during the airflow.

An important diabatic process is cloud radiative effect. We analysed four relevant variables: total column liquid water, total column ice, total column water (sum of vapour, liquid, and ice), and total cloud fraction (including low-, middle-, and high-level clouds) over Helsinki, Kazan, Moscow and Archangelsk. Comparing the periods 1979-1997 and 1998-2015, there are predominantly increasing values for all these variables both when averaged over all airmass origins and when calculated separately for southeasterly airmass origins (**Supplementary Table S3**). As subsidence typically favours reduced cloud cover (van der Dussen et al., 2016), the results for increased cloudiness are

consistent with the decreased subsidence in cases of southeasterly airmass origin. Note that we address air temperatures at 1 km altitude. Hence, there is not such a marked wintertime warming effect of clouds via increased downward longwave radiation as there would be at the surface. For airmass origins other than southeasterly, the changes in adiabatic subsidence heating were smaller, with mean values ranging from a decrease of 0.7ºC in Archangelsk to an increase of 0.1ºC in Helsinki.

In addition to the anomalous cooling cases, the strongest warmings for certain airmass origins deserve attention (**Figure 11)**. In Glasgow, the airmasses of southeasterly origin have become 1.8 ºC warmer. This is due to both thermodynamic and dynamic effects: warming under all circulation patterns and an increased occurrence of the warmest pattern, EAWR (with a 500 hPa high over British Isles), during southeasterly flow (**Figure 12**; **Table 4**). In Hammerfest, warming has been strongest in cases of northwesterly and northeasterly airmass origins. This is mostly related to overall warming during NAO-, EAWR, NAO+ and DIPOL (**Figure 12**), which has dominated over the effects of increasing occurrence of the cold NAO- and DIPOL patterns (**Table 4**). Also the occurrence of the relatively warm SCA+ pattern has increased during northeasterly and northwesterly flows. The strongest overall warming has occurred in Bucharest (**Figure 11**), where all five patterns have become warmer (**Figure 12**). Considering dynamical effects, during southeasterly flows the strongly increased occurrence of the by far warmest NAO+ pattern has dominated. During southwesterly flows, the decreased occurrence of the cold EAWR pattern has contributed to warming. In contrast, the occurrence of the even colder SCA+ pattern has increased, but its effect has been partly compensated by the strong thermodynamic warming of the pattern. During northeasterly flows, dynamic effects supporting warming include the decreased occurrence of the cold SCA+ pattern and increased occurrence of NAO-, which is associated with high temperatures in Bucharest.

4. Discussion and Conclusions

Our study investigated multiple approaches to illuminate the factors contributing to regional temperature variations in Europe, how temperatures are changing in the recent era of Arctic amplification, and which factors are responsible for the changes. Analysis methods include spatial and lagged correlations, two types of pattern analysis, back trajectories of airmass origins, and a separation of dynamic and thermodynamic contributions to temperature changes.

The analyses revealed several new quantitative findings for the spatial relationship between regional temperature variations in Europe and the Arctic, summarized in the bullet points below:

- Statistical relationships between the number of cold days in CE and NE and warm days in Greenland have become consistently stronger during the AA era, as have relationships between cold days in SE and EE and warm days in the Barents-Kara seas region (**Table 2**).

Extreme cold winter events, at least four days long, in WE, CE and NE are significantly related to positive temperature anomalies in the Greenland / Baffin region, whereas in SE and EE extremely cold winter events are associated with both the Greenland / Baffin region and the Barents-Kara seas area (**Figure 3**). In addition, inter-annual variations in Europe are associated with those in the Arctic, seen as significant correlations between the number of cold days per winter in Europe and the number of warm days per winter in the Arctic (**Table 2**), with basically the same geographic relationships between the European and Arctic regions as in the case of synoptic-scale extreme events. Both the synoptic-scale (**Table 1**) and interannual (**Table 2**) relationships are stronger during the period of AA. While these results do not prove causality, they are qualitatively consistent with previous results suggesting that AA favours cold winter events in mid-latitudes, including Europe (Yang and Christensen, 2012; Grassi et al., 2013; Cohen et al., 2014; Koenigk et al., 2016; Screen, 2017).

The large-scale circulation analyses, based on SOM and cluster methods, demonstrated close associations of both NAO and SCA with European winter temperatures (**Figures 6 and 10**), in line

with previous studies (e.g., Yiou and Nogaj, 2004). The cluster method also highlighted the role of EAWR and DIPOL patterns.

● Under the occurrence of NAO- and SCA+, European temperature anomalies were mostly collocated with convergence of dry static energy transport, whereas under NAO+ and SCA- the temperature anomalies were to some extent collocated with convergence of latent heat transport (**Table 3**).

We interpret these relationships to mean that NAO+ and SCA- are associated with stronger westerly winds that advect moist airmasses from the Atlantic to Europe, resulting in a strong effect of latent heat transport on T2m. In contrast, NAO- and SCA+ favour more meridional circulation types, during which dry static energy transport dominates. Also, under NAO- and SCA+, European winter temperatures are typically low (**Figure 6**), which limits the maximum possible latent heat content of the airmass. Spatial correlations between T2m anomalies and the sum of latent heat and dry static energy convergences are in most cases strongly negative, but do not reach -1, as T2m anomalies are also affected by local factors not controlled by large-scale transport. Although the magnitude of latent heat transport divergence is mainly smaller than that of the dry-static energy transport divergence, it sometimes, mostly under NAO- and SAC+, has a larger effect on near-surface temperatures, as the latent heat transport also enhances the local greenhouse effect by increasing the local humidity and cloudiness (Graversen and Burtu, 2016).

● The statistically significant lagged relationships between Arctic temperature anomalies and large-scale circulation patterns (**Figure 7**) was an important finding. The most robust result was that SCA- and NAO+ are typically preceded by a long period, up to 3 months, of negative temperature anomaly averaged over the circumpolar Arctic north of 70^{o}N.

As NAO+ and SCA- on average coincide with a strong zonal flow (Bueh and Nakamura, 2007; Hurrell and Deser, 2009), this result aligns with previous findings that AA is associated with weaker

zonal winds (Francis and Vavrus, 2012; 2015; Davy et al., 2018). Interestingly, there is a more robust relationship between Arctic temperature anomalies and NAO/SCA patterns (longer and more continuous periods of statistically significant temperature anomalies) in the case of an abnormally cold Arctic at time scales of 1 to 90 days than in the case of a warm Arctic, which has received more attention as AA has intensified (Pedersen et al., 2016, Vavrus, 2018). The results presented in **Figure 7** can be exploited to improve seasonal forecasting, an endeavour that warrants further study.

- Comparing periods 1998-2015 and 1979-1997, both the SOM and cluster methods indicated statistically significant increases in the occurrence of SCA+ in December and January and NAO- in February and March. In general, SCA+ and NAO- favour cold winter weather in Europe. Despite the overall warming trend, SCA+ is associated with remarkable winter cooling in northeastern Europe (**Figure 8**).

The changes observed are potentially associated with the sea-ice decline in the Barents and Kara seas, favouring SCA+ in early winter (Jaiser et al., 2012; Crasemann et al., 2017), and enhancement of the climatological planetary wavenumber 1 through constructive wave interference (Smith et al, 2010; Hoshi et al., 2019 and references therein). According to Jaiser et al. (2013; 2016), this process is followed by an increased flux of wave activity propagating to the stratosphere, which may finally lead to a tropospheric Arctic Oscillation response through downward stratosphere-to-troposphere coupling mechanisms, further strengthening the Siberian high (Cohen et al., 2014; Kidston et al., 2015). The Arctic Oscillation response manifests over the North Atlantic-Eurasian region as an increased frequency of occurrence of NAO- in late winter. Some modelling studies have suggested that the strengthening of the Siberian high is due to inter-annual and decadal variability (McCusker et al., 2016), but experiments applying models with a well-resolved stratosphere show a robust link with AA (Wu and Smith 2016; Zhang et al., 2019).

● Comparing periods 1979-1997 and 1998-2015, in cases of southeasterly airmass origin, cooling at 1 km altitude occurred in Kazan, Moscow, Helsinki, and Archangelsk, in particular in March.

In these cities, a major contributing cooling effect was the decrease of subsidence along the airmass trajectories. Considering horizontal large-scale circulation, the cooling was associated with dynamic factors (changes in pattern frequency) that dominated over the overall thermodynamic (pattern-wide) warming. Circulation patterns associated with low temperatures, particularly the NAO- and related southeasterly flow, became more common during 1998-2015, while patterns associated with high temperatures, particularly NAO+, became rarer. The winter-average T2m change in Kazan, Archangelsk, and Moscow was dominated by cooling in March, with monthly mean values of -1.8, -1.3, and -0.8 K, respectively. This cooling was due primarily to the significantly increased occurrence of NAO- (dynamic effect). These results are consistent with the previously discussed strengthening of the Siberian high in March. In general, our results are in accordance with previous studies demonstrating the major role of dynamic effects in decadal-scale variations in mean and extreme air temperatures (Corti et al., 1999; Yiou and Nogaj, 2004).

During the period of recent AA, airmasses originating from the Arctic have, by definition, become generally warmer. However, Arctic warming has also indirectly affected Europe in winter. An increased frequency in long-duration events associated with NAO- (**Figure 9**) favours persistent cold winter weather in Europe, and a decrease of those events, associated with NAO+, favours less persistent warm winter periods. An increased persistence is favoured by the finding that NAO- patterns have increased more than NAO+ patterns.

Notwithstanding, comparing the period 1998-2015 against 1979-1997, European winters have generally warmed (**Figures 8, 11, and 12b; Supplementary Figure S2)**

Finally, we acknowledge that European winter temperatures are also affected by other factors than those explicitly discussed above. Such factors include atmosphere-ocean coupling in the tropics and subtropics; shifting large-scale ocean temperature patterns; radiative forcings by greenhouse gases, aerosols, and ozone; as well as internal variability. The projected future amplification of climate warming in the upper tropical troposphere would tend to strengthen the sub-tropical jet stream and shift it farther north, acting against the effects of Arctic amplification (McGraw and Barnes, 2016; Zappa et al., 2018). In addition, many studies have identified linkages between SST variations in the tropical and/or northern Atlantic Ocean and weather patterns in Europe (Marshall et al., 2001; Cassou et al., 2004; Davini et al., 2015; Hall et al., 2015; Yeager and Robson, 2018). Furthermore, the Pacific Decadal Oscillation (PDO) potentially has remote effects on European winters (Trenberth and Fasullo, 2013; Vihma et al., 2014). On multi-decadal time scales, the Atlantic Multi-decadal Variability (AMO) also plays important role (Keenlyside and Omrani, 2014; Peings and Magnusdottir, 2014). In any case, the effects of all factors, except the direct raditative forcing, are implicitly included in the reanalysis-based large-scale circulation patterns objectively analysed here.

North Atlantic variability will dominate the day-to-day and year-to-year fluctuations in future European winter temperatures. However, as greenhouse gases accumulate further and Arctic amplification intensifies, our findings suggest that Arctic influences on European winter weather may intensify, perhaps leading to more unusual and persistent weather events.

Acknowledgements

The authors were supported by the following funding agencies and grants: TV, AK, and NT by the Academy of Finland (contracts 317999, 286298, and 294120), JF and NS by the NSF/ARCSS grant 1304097 and support from the Woods Hole Research Center, PU by the EU MCSA grant 707262 – LAWINE, LC by the Research Council of Norway (231322/F20), JEO by the Arctic Research Project of the NOAA Global Ocean Monitoring and Observation Program (PMEL contribution # xxxx), DH by the German Federal Ministry for Education and Research (BMBF, grant 03F0777A, project QUARCCS), KD by the SFB/TR172 "Arctic Amplification: Climate Relevant Atmospheric and Surface Processes, and Feedback Mechanisms (AC)³" funded by the Deutsche Forschungsgemeinschaft (DFG), and RG via computational resources at the University of Tromsø provided by the Norwegian Metacenter for Computational Science (NOTUR) under the project nn9348k. This is PMEL contribution 4771. We acknowledge The World Climate Research Programme's Climate & Cryosphere project for providing funding support for a discussion workshop. The ECMWF is acknowledged for providing us with the ERA-Interim reanalysis data.

References

Barnston, A.G., Livezey, R.E. (1987). Classification, seasonality and persistence of low frequency atmospheric circulation patterns. Mon. Weather Rev. 115, 1083–1126.

Buckley, M. W. and J. Marshall (2016), Observations, inferences, and mechanisms of Atlantic Meridional Overturning Circulation variability: A review, Rev. Geophys., 54, 5–63, doi:10.1002/2015RG000493.

Bueh C, Nakamura H (2007) Scandinavian pattern and its climate impact. Q J Royal Meteorol Soc 133:2117–2131.

Cassou, C., Terray, L., Hurrell, J. W., & Deser, C. (2004) North Atlantic winter climate regimes: Spatial asymmetry, stationarity with time, and oceanic forcing. J.Climate, 17, 1055-1068. Doi:10.1175/1520-0442(2004)017<1055:NAWCRS>2.0.CO;2

Cohen, J., and Co-authors, 2014: Recent Arctic amplification and extreme mid-latitude weather. Nat. Geosci., 7, 627–637, doi:10.1038/ngeo2234.

Cohen, J., J.A. Francis, and K. Pfeiffer, Winter 2015/16, 2017: A turning point in ENSO-based seasonal forecasts. Oceanography, 30(1), https://doi.org/10.5670/ oceanog.2017.115.

Cohen, J., K. Pfeiffer, and J.A. Francis, 2018: Warm Arctic episodes linked with increased frequency of extreme winter weather in the United States. Nat. Comm., 9, doi:10.1038/s41467-018-02992-9.

Corti, S., F. Molteni, and T. N. Palmer (1999), Signature of recent climate change in frequencies of natural atmospheric circulation regimes, Nature, 398, 799– 802.

Coumou, D., V. Petoukhov, S. Rahmstorf, S. Petri and H-J. Schellnhuber (2014). Quasi-resonant circulation regimes and hemispheric synchronization of extreme weather in boreal summer, Proc. Nat. Ac. Sci., 111(34), p.12331-12336.

Crasemann B, Handorf D, Jaiser R, Dethloff K, Nakamura T, Ukita J., and Yamazaki K 2017 Can preferred atmospheric circulation patterns over the North-Atlantic-Eurasian region be associated with arctic sea ice loss? Polar Sci. 14 9–20.

Dee DP, Uppala SM, Simmons AJ, Berrisford P, Poli P, Kobayashi S, Andrae U, Balmaseda MA, Balsamo G, Bauer P, Bechtold P, Beljaars ACM, van de Berg L, Bidlot J, Bormann N, Delsol C, Dragani R, Fuentes M, Geer AJ, Haimberger L, Healy SB, Hersbach H, Hólm EV, Isaksen L, Kållberg P, Köhler M, Matricardi M, McNally AP, Monge-Sanz BM, Morcrette J-J, Park B-k, Peubey C, de Rosnay P, Tavolato C, Thépaut J-N, Vitart F. 2011. The ERA-Interim reanalysis: configuration and performance of the data assimilation system.Q. J. R. Meteorol. Soc., **137**: 553-597, DOI: 10.1002/qj.828

Davini P, von Hardenberg J, Corti S (2015) Tropical origin for the impacts of the Atlantic Multidecadal Variability on the Euro-Atlantic climate. Environ Res Lett 10:094010. doi: 10.1088/1748-9326/10/9/094010

Davy R, Chen L, Hanna E. (2018). Arctic amplification metrics. Int. J. Climatol., 38: 4384–4394. https://doi.org/10.1002/joc.5675

Dawson, A. and T. N. Palmer (2015) Simulating weather regimes: impact of model resolution and stochastic parameterization. Clim. Dyn. 44, 2177-2193. Doi: 10.1007/s00382-014-2238-x.

Deser, C., L. Sun, R. A. Tomas, and J. Screen (2016), Does ocean coupling matter for the northern extratropical response to projected Arctic sea ice loss?, Geophys. Res. Lett., 43, doi:10.1002/2016GL067792.

Francis, J.A., N. Skific, S.J. Vavrus, 2018: North American weather regimes are becoming more persistent: Is Arctic amplification a factor? Geophys. Res. Lett., in review.

Francis, J.A. (2017). Why are Arctic linkages to extreme weather still up in the air? Bull. Amer. Meteoro. Soc., 98, 2551–2557.

Francis, J.A. and N. Skific, 2015: Evidence Linking Rapid Arctic Warming to Mid-latitude Weather Patterns. Philosophical Transactions of the Royal Society A 373, doi:10.1098/rsta.2014.0170.

Grassi B, Redaelli G, Visconti G (2013) Arctic sea-ice reduction and extreme climate events over the Mediterranean region. J Clim., doi:10.1175/JCLI-D-12-00697.1

Graversen, R.G. (2006). Do changes in mid-latitude have any impact on the Arctic surface air temperature trend? J. Clim., 19, 5422-5438.

Graversen and Burtu (2016). Arctic amplification enhanced by latent energy transport of atmospheric planetary waves. Q. J. R. Meteorol. Soc., 142, 2046—2054.

Hall R, Erdélyi R, Hanna E, Jones JM, Scaife AA. 2015. Drivers of North Atlantic polar front jet stream variability. Int. J. Climatol. 35: 1697–1720, doi: 10.1002/joc.4121.

Handorf, D., R. Jaiser, K. Dethloff, A. Rinke, and J. Cohen (2015), Impacts of Arctic sea ice and continental snow cover changes on atmospheric winter teleconnections, Geophys. Res. Lett., 42, 2367–2377, doi:10.1002/2015GL063203.

Hanna, E., and T.E. Cropper (2017) North Atlantic oscillation. Oxford Research Encyclopedia of Climate Science, http://climatescience.oxfordre.com/view/10.1093/acrefore/9780190228620.001.0001/acrefore-9780190228620-e-22

Hanna, E., Cropper, T. E., Hall, R. J. & Cappelen, J. (2016). Greenland Blocking Index 1851–2015: a regional climate change signal. Int. J. Climatol., 36: 4847–4861 http://doi.org/brqf.

Hanna, E., R.J. Hall, T.E. Cropper, T.J. Ballinger, L. Wake, T. Mote, J. Cappelen (2018) Greenland blocking index daily series 1851-2015: analysis of changes in extremes and links with North Atlantic and UK climate variability and change. Int. J. Climatol., doi: 10.1002/joc.5516.

Hanna, E., R.J. Hall, J.E. Overland (2017). Can Arctic warming influence UK extreme weather? Weather, 72, 346-352.

Hewitson, B, Crane, R. (2002). Self-organizing maps: applications to synoptic climatology. Clim Res 22(1):13–26. doi:10.3354/ cr022013.

Hoshi, K., Ukita, J., Honda, M., Nakamura, T., Yamazaki, K., Miyoshi, Y., & Jaiser, R. (2019). Weak stratospheric polar vortex events modulated by the Arctic sea-ice loss. Journal of Geophysical Research: Atmospheres, 124. https://doi.org/10.1029/2018JD029222.

Hurrell, J. W., and C. Deser (2009). North Atlantic climate variability: The role of the North Atlantic Oscillation. J. Mar. Sys., 78, 28–41.

Hurrell, J. W., Y. Kushnir, G. Ottersen, and M. (2003). An Overview of the North Atlantic Oscillation, 134, American Geophysical Union, https://doi.org/10.1029/134GM01.

IPCC, 2012: Managing the Risks of Extreme Events and Disasters to Advance Climate Change Adaptation. A Special Report of Working Groups I and II of the Intergovernmental Panel on Climate Change [Field, C.B., V. Barros, T.F. Stocker, D. Qin, D.J. Dokken, K.L. Ebi, M.D. Mastrandrea, K.J. Mach, G.-K. Plattner, S.K. Allen, M. Tignor, and P.M. Midgley (eds.)]. Cambridge University Press, Cambridge, UK, and New York, NY, USA, 582 pp.

Keenlyside, N. and Omrani, N.-E. (2014). Has a warm North Atlantic contributed to recent European cold winters? Environmental Research Letters, 9(6), 061001.

Kim, B.-M., Son, S.-W., Min, S.-K., Jeong, J.-H, Kim, S.-J., Zhang, X., Shim, T., and Yoon, J.-H. (2014). Weakening of the stratospheric polar vortex by Arctic sea-ice loss. Nat. Commun. 5, 4646.

Kohonen T. (2001). Self-Organizing Maps. Springer, Berlin, 501 p.

Kolstad, E. W., Bracegirdle, T. J., and Seierstad, I. A. (2009). Marine coldair outbreaks in the North Atlantic: Temporal distribution and associations with large-scale atmospheric circulation, Clim. Dynam., 33, 187–197.

Kornhuber, K., V. Petoukhov, D. Karoly, S. Petri, S. Rahmstorf, and D. Coumou (2017). Summertime planetary wave resonance in the Northern and Southern Hemispheres. J. Clim, https://doi.org/10.1175/JCLI-D-16-0703.1.

Kretschmer, M., Coumou, D., Donges, J. F. & Runge, J. (2016). Using Causal Effect Networks to analyze different Arctic drivers of mid-latitude winter circulation. J. Clim., doi:10.1175/JCLI-D-15-0654.1

Kug, J.-S., J-H. Jeong, Y.-S. Jang, B.-M. Kim, C. K. Folland, S.-K. Min, and S.-W. Son (2015). Two distinct influences of Arctic warming on cold winters over North America and East Asia. Nature Geosci., DOI: 10.1038/NGEO2517.

Koenigk, T., M. Caian, G. Nikulin, and S. Schimanke (2016). Regional Arctic sea ice variations as predictor for winter climate conditions. Clim Dyn (2016) 46:317–337. DOI 10.1007/s00382-015-2586-1.

Lim, Y.-K. (2015). The East Atlantic/West Russia (EA/WR) teleconnection in the North Atlantic: Climate impact and relation to Rossby wave propagation. Climate Dyn., 44, 3211–3222, https://doi.org/10.1007/s00382-014-2381-4.

Mann, M. E., S. Rahmstorf, K. Kornhuber, B. A. Steinman, S. K. Miller, and D. Coumou (2017). Influence of anthropogenic climate change on planetary wave resonance and extreme weather events. Sci. Rep., 7, 45242, doi:10.1038/srep45242.

Marshall J, Johnson H, Goodman J (2001) A study of the interaction of the North Atlantic Oscillation with ocean circulation. J Clim 14:1399–1421.

Marshall, J., Kushnir, Y., Battisti, D., Chang, P., Czaja, A., Dickson, R., Hurrell, J., McCartney, M., Saravanan, R., Visbeck, M., (2001) North Atlantic climate variability: phenomena, impacts and mechanisms. Int. J. Clim. 21, 1863–1898.

Masato, G., T. Woollings, and B. J. Hoskins (2014), Structure and impact of atmospheric blocking over the Euro-Atlantic region in present-day and future simulations, Geophys. Res. Lett., 41, 1051–1058, doi:10.1002/2013GL058570.

McCusker, K. E., J. C. Fyfe, and M. Sigmond (2016), Twenty-five winters of unexpected Eurasian cooling unlikely due to Arctic sea ice loss. Nat. Geosci., 838–842, https://doi.org/10.1038/ngeo2820.

McGraw, M. and Elizabeth A. Barnes, 2016: Seasonal Sensitivity of the Eddy-Driven Jet to Tropospheric Heating in an Idealized AGCM. J. Climate, 29, doi:10.1175/JCLI-D-15-0723.1.

Munich Re (2018), NatCatService, https://www.munichre.com/topics-online/en/climate-change-and-natural-disasters/climate-change/climate-change-heat-records-and-extreme-weather.html

Nakamura, T., K. Yamazaki, K. Iwamoto, M. Honda, Y. Miyoshi, Y. Ogawa, and J. Ukita (2015), A negative phase shift of the winter AO/NAO due to the recent Arctic sea-ice reduction in late autumn, J. Geophys. Res. Atmos., 120, 3209–3227, doi:10.1002/2014JD022848.

Overland, J. E., K. Dethloff, J. A. Francis, R. J. Hall, E. Hanna, S.-J. Kim, J. A. Screen, T. G. Shepherd, and T. Vihma (2016), The Melting Arctic and Midlatitude Weather Patterns: Forced Chaos and a Way Forward. Nature Climate Change, DOI: 10.1038/NCLIMATE3121

Overland, J., J. Francis, R. Hall, E. Hanna, S.-J. Kim, and T. Vihma (2015). The Melting Arctic and Mid-latitude Weather Patterns: Are They Connected? Journal of Climate, 28, 7917-7932, DOI: 10.1175/JCLI-D-14-00822.1.

Overland, J.E., and M. Wang (2018). Resolving future Arctic/midlatitude weather connections. Earth's Future, 6(8), 1146–1152, doi: 10.1029/2018EF000901,

Overland, J.E., M. Wang, and J.E. Box (2019). An integrated index of recent pan-Arctic climate change. Environ. Res. Lett., doi: 10.1088/1748-9326/aaf665.

Pedersen, R. A., I. Cvijanovic, P. L. Langen, and B. M. Vinther, 2016: The impact of regional Arctic sea ice loss on atmospheric circulation and the NAO. J. Climate, 29, https://doi.org/10.1175/JCLI-D-15-0315.1.

Peings, Y. and Magnusdottir, G. (2014) Forcing of the wintertime atmospheric circulation by the multidecadal fluctuations of the North Atlantic Ocean. Environmental Research Letters, 9(3), 034018.

Petoukhov, V., S. Rahmstorf, S. Petri and H. J. Schellnhuber (2013). Quasiresonant amplification of planetary waves and recent Northern Hemisphere weather extremes. Publ. Nat. Acad. Sci., 110 (14) 5336-5341. https://doi.org/10.1073/pnas.1222000110.

Saha S, Moorthi S, Pan H-L, Wu X, Wang J, et al. (2010). The NCEP climate forecast system reanalysis. Bull. Am. Meteorol. Soc. 91: 1015–1057, doi: 10.1175/2010BAMS3001.1.

Sato, K., Inoue, J. & Watanabe, M. (2014). Influence of the Gulf Stream on the Barents Sea ice retreat and Eurasian coldness during early winter. Environ. Res. Lett. 9, 084009.

Screen, J.A. (2017). Simulated atmospheric response to regional and pan-Arctic sea ice loss, J. Clim., 30, 3945-3962.

Screen, J. A., 2014: Arctic amplification decreases temperature variance in northern mid- to high-latitudes. Nat. Climate Change, 4, 577–582, doi:10.1038/nclimate2268.

Screen JA, Deser C, Simmonds I, Tomas R. (2014) Atmospheric impacts of Arctic sea-ice loss, 1979-2009: separating forced change from atmospheric internal variability, Clim. Dyn., 43, 333-344, DOI:10.1007/s00382-013-1830-9.

Serreze MC, Barrett AP, Cassano JJ (2011) Circulation and surface controls on the lower tropospheric temperature field of the Arctic. J Geophys Res 116:D07104

Singarayer J, Bamber J, Valdes P (2006) Twenty-first-century climate impacts from a declining Arctic sea ice cover. J Clim 19:1109–1125.

Smith, D., N.J. Dunstone, A.A. Scaife, E.K. Fiedler, D. Copsey, S.C. Hardiman (2017) Atmospheric response to Arctic and Antarctic sea ice: the importance of ocean-atmosphere coupling and the background state. J. Clim. 30, 4547-4565.

Straus, D. M., S. Corti, F. Molteni (2007) Circulation regimes: chaotic variability versus SST-forced predictability. J. Clim. 20, 2251-2272. Doi:10.1175/JCLI4070.1.

Stull, R. B. (2001). An Introduction to Boundary Layer Meteorology (1st ed.). Kluwer Academic Publishers, 670 pp.

Trenberth, K. E. (1991). Climate diagnostics from global analysis: Conservation of mass in ECMWF analysis. J. Clim., 4, 707-721.

Trenberth K E, Fasullo J T. (2013). An apparent hiatus in global warming? Earth's Future, doi:10.1002/2013EF000165.

van der Dussen, J. J., de Roode, S. R., and Siebesma, A. P. (2016). How large-scale subsidence affects stratocumulus transitions, Atmos. Chem. Phys., 16, 691-701, https://doi.org/10.5194/acp-16-691-2016.

Vautard, R. (1990). Multiple weather regimes over the North Atlantic: Analysis of precursors and successors. Monthly weather review, 118(10), 2056-2081.

Vavrus, S.J., F. Wang, J. Martin, J. Francis, Y. Peings, and J. Cattiaux, 2017: Changes in North American atmospheric circulation and extreme weather: Influence of Arctic amplification and northern hemisphere snow cover. J. Climate, 4317-4333, doi: 10.1175/JCLI-D-16-0762.1.

Vavrus, S. J. (2018). The influence of Arctic amplification on mid-latitude weather and climate. Current Climate Change Reports. https://doi.org/10.1007/s40641-018-0105-2

Vihma, T. (2014). Effects of Arctic sea ice decline on weather and climate: A review. Surv. Geophys., 35, 1175–1214, doi:10.1007/s10712-014-9284-0.

Vihma, T. (2017). Weather extremes linked to interaction of the Arctic and mid-latitudes, In: Climate Extremes: Mechanisms and Potential Prediction, Wang, S.-Y., et al. (Eds.), Geophysical Monograph Series, 226, American Geophysical Union, p. 39-49.

Vihma, T., B. Cheng, P. Uotila, Wei, L., and Qin, T. (2014). Linkages between Arctic sea ice cover, large-scale atmospheric circulation, and weather and ice conditions in the Gulf of Bothnia, Baltic Sea, Adv. Polar Sci. 25, 4,289-299, doi: 10.13679/j.advps.2014.4.00289.

Wu Y, Smith KL. Response of Northern Hemisphere midlatitude circulation to Arctic amplification in a simple atmospheric general circulation model. J Clim. 2016;29:2041–58, https://doi.org/10.1175/JCLI-D-15-0602.1

Yang S, Christensen JH (2012) Arctic sea ice reduction and European cold winters in CMIP5 climate change experiments. Geophys Res Lett 39:L20707.

Yeager SG, Robson JI (2017) Recent progress in understanding and predicting Atlantic decadal climate variability. Curr Clim Chang Reports 3(2):112–127. https://doi.org/10.1007/s40641-017-0064-z

Yiou, P., and M. Nogaj (2004), Extreme climatic events and weather regimes over the North Atlantic: When and where?, Geophys. Res. Lett., 31, L07202, doi:10.1029/2003GL019119.

Yue S, Wang C. (2004). The Mann-Kendall test modified by effective sample size to detect trend in serially correlated hydrological series. Water resources management 18(3): 201-218.

Zappa, G., Pithan, F., & Shepherd, T. G. (2018). Multimodel evidence for an atmospheric circulation response to Arctic sea ice loss in the CMIP5 future projections. Geophysical Research Letters, 45. https://doi.org/10.1002/2017GL076096

Zappa, G., and T. G. Shepherd (2017), Storylines of atmospheric circulation change for European regional climate impact assessment, J Climate, 30, 6561{6577, doi:10.1175/JCLI-D-16-0807.1.

Zeng, J., T. Matsunaga, H. Mukai (2010). METEX – A flexible tool for air trajectory calculation, Environmental Modelling & Software, 25, 607-608, doi:10.1016/j.envsoft.2008.10.015.

Zhang, P., Wu, Y., Simpson, I. R., Smith, K. L., Zhang, X., De, B., and Callaghan, P. (2019). A stratospheric pathway linking a colder Siberia to Barents-Kara Sea sea ice loss. Science Advances, 4, eaat6025, DOI: 10.1126/sciadv.aat6025

Table 1. Number of cold events in each European region that are preceded by or synchronous with warm Arctic (+1.75 SD criteria) and GBI (+2 SD criteria) events.

	Trend retained				Detrended			
	Warm Arctic		GBI		Warm Arctic		GBI	
Region	1979-1997	1998-2015	1979-1997	1998-2015	1979-1997	1998-2015	1979-1997	1998-2015
Western Europe		1	1	3				3
Southern Europe		1	1	1		1		1
Central Europe	1	1	1	2	1			2
Eastern Europe		5		1		4		2
Northern Europe		2				1	1	3
Total	1	10	3	7	1	6	1	11

Table 2. Correlation coefficients between the number of extremely warm days per winter (+1.75SD, without 4-day criterion) in the two Arctic areas and the number of extremely cold days per winter (-2SD, without 4-day criterion) in five European areas. Numbers in bold denote significant correlation with a 95% confidence. P1 indicates period of 1979-2015; P2 is 1979-1997; and P3 is 1998-2015.

Europe region	**Greenland/Baffin (warm)**			**Barents-Kara sea (warm)**		
	P1	P2	P3	P1	P2	P3
WE (cold)	**0.50**	**0.50**	**0.51**	-0.01	0.10	0.26
CE (cold)	**0.36**	0.33	**0.51**	0.31	0.24	0.33
SE (cold)	0.10	0.03	0.16	**0.36**	0.17	**0.78**
NE (cold)	**0.47**	0.38	**0.58**	0.13	0.27	-0.13
EE (cold)	0.17	0.17	0.18	**0.34**	0.34	**0.53**

Table 3. Spatial correlation coefficient between energy transport divergence and T2m anomalies in Europe (35-70ºN, 10ºW-60ºE) for the six most common SOM nodes and for the entire data set.

	Node 1	**Node 3**	**Node 4**	**Node 9**	**Node 10**	**Node 12**
	SCA-	**NAO+**	**NAO+**	**NAO-**	**NAO-**	**SCA+**
Latent heat	-0.48	-0.32	-0.47	-0.31	-0.01	-0.25
Dry-static energy	-0.33	-0.02	-0.28	-0.82	-0.71	-0.63
Total = latent heat + dry static energy	-0.51	-0.26	-0.53	-0.86	-0.79	-0.81

Table 4. Occurrence (in %) of large-scale circulation patterns, based on cluster analysis, in conditions of airmass origins from the southeast (SE), southwest (SW), and northeast (NE) for selected cities.

		C1 = NAO+		**C2 = EAWR**		**C3 = SCA+**		**C4 = NAO-**		**C5 = DIPOL**	
Origin	City	1979-1997	1998-2015	1979-1997	1998-2015	1979-1997	1998-2015	1979-1997	1998-2015	1979-1997	1998-2015
SE	Hel	15	10	7	8	40	45	21	26	16	11
SE	Arc	22	14	11	13	29	31	22	25	16	18
SE	Kaz	28	18	7	6	28	37	15	21	22	17
SE	Mos	21	13	8	7	38	39	17	23	16	17
SE	Gla	7	5	30	36	25	24	29	29	8	6
SE	Buc	12	11	19	12	35	42	20	12	14	13
SW	Buc	34	33	18	12	11	16	22	23	15	17
NE	Buc	16	13	22	25	33	28	15	19	14	16
NE	Ham	23	18	25	15	8	10	27	29	18	27
NW	Ham	24	22	22	19	12	13	20	20	22	26

Figures

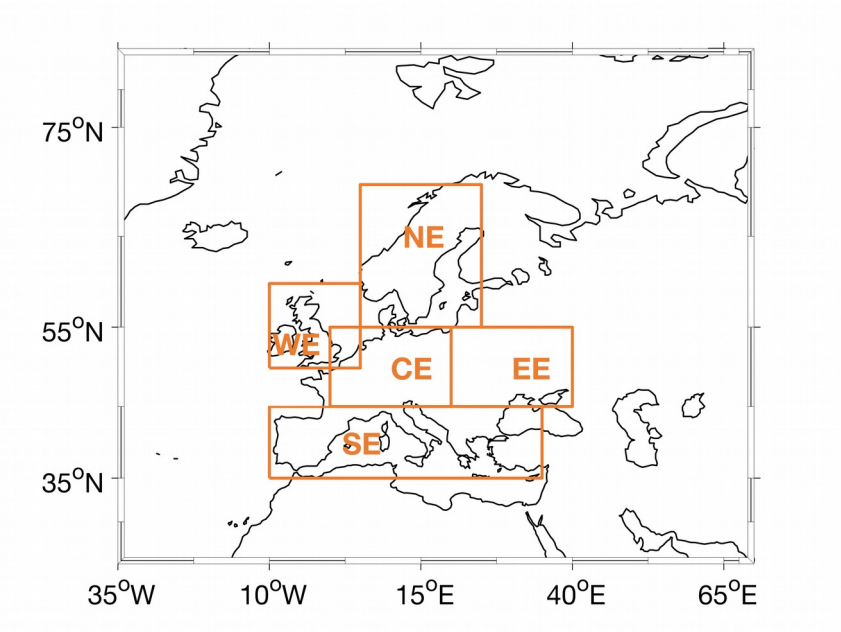

Figure 1. Map of five European areas. **CE: central Europe 45°N-55°N, 0°-20°E; SE: southern Europe 35°N-45°N, 10°W-35°E; NE: northern Europe 55°N-70°N, 5°E-25°E; WE: western Europe 50°N-60°N, 10°W-5°E; EE: eastern Europe 45°N-55°N, 20°E-40°E**

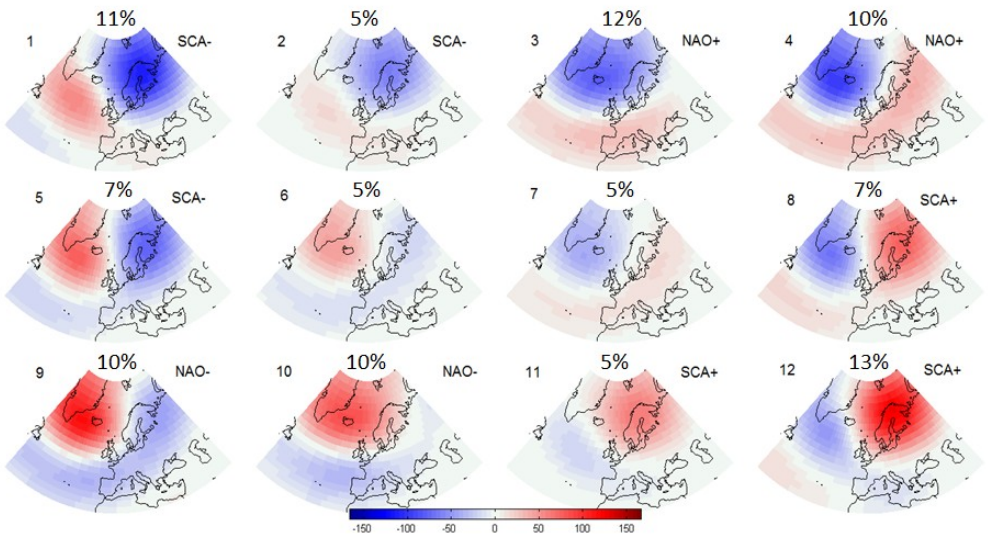

Figure 2. Self-Organizing Maps (SOMs) generated using 500 hPa height anomalies from ERA-Interim reanalysis, 1979-2015. The patterns are numbered from 1 to 12, and most are named after the large-scale circulation patterns they resemble. The percentages above each pattern denote their relative frequency of occurrence.

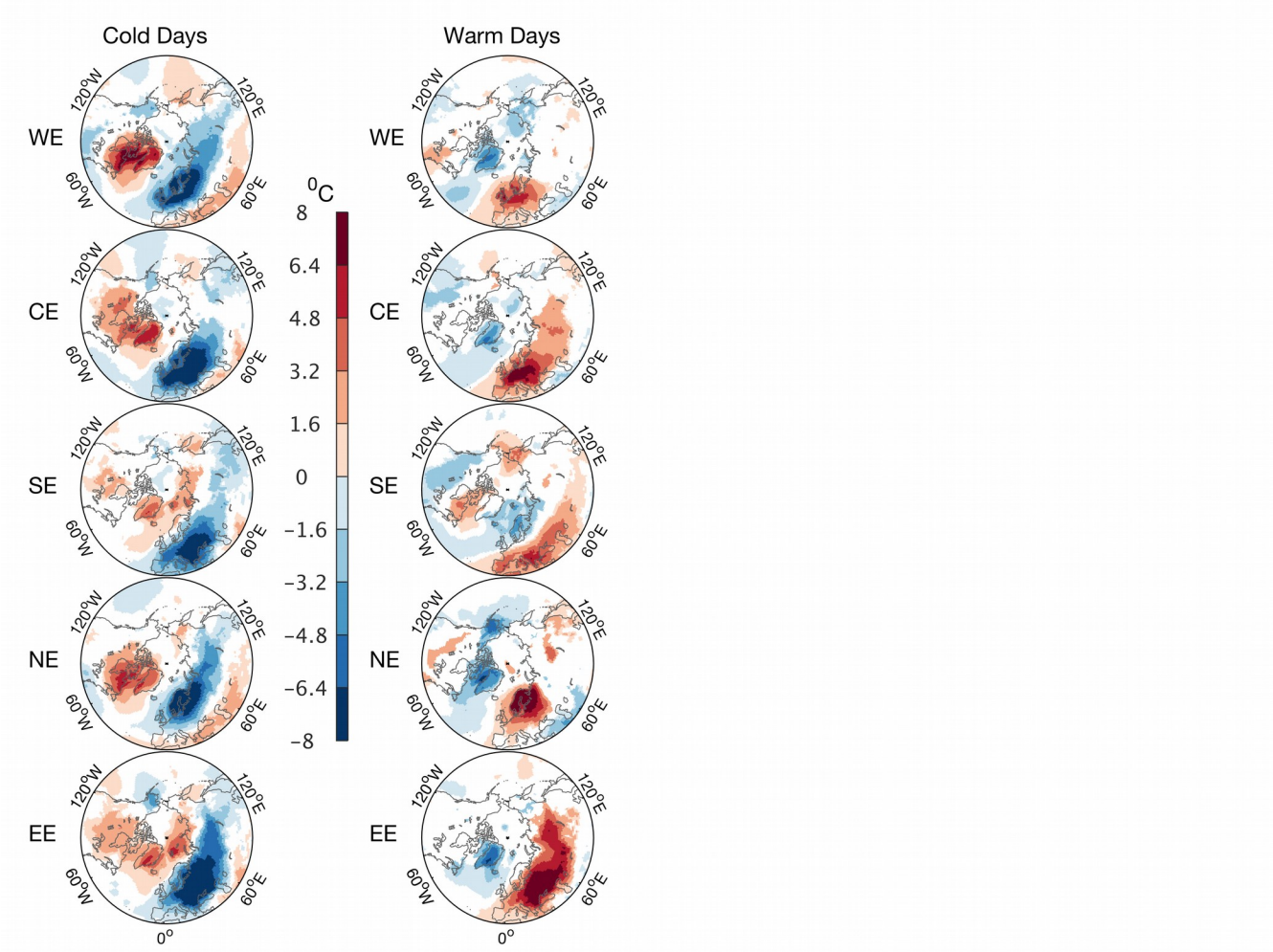

Figure 3. Composite maps of the Northern Hemisphere T2m anomalies related to (1ST column) extremely cold events (-2SD as threshold) and (2nd column) extremely warm events (+1.75SD as threshold) in western (WE), central (CE), southern (SE), northern (NE), and eastern Europe (EE) during winters (DJFM) 1979-2015. The colour shadings denote the areas with significant (95% confidence) differences between the anomalous events and the normal events (less than +1.75SD and greater than -2SD).

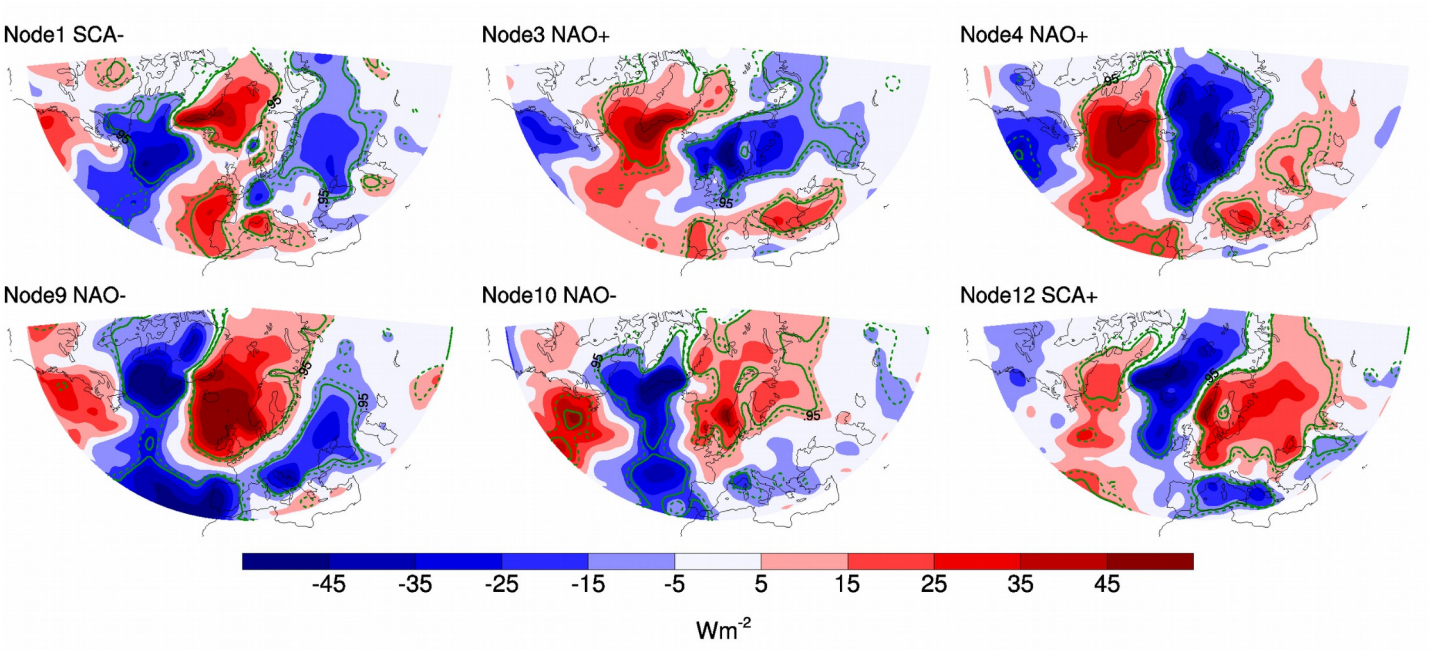

Figure 4. Winter (DJFM) anomalies of the divergence of vertically-integrated latent heat transport mapped to the six most common nodes of the SOM matrix in Figure 2. Anomalies are relative to monthly climatology of 1979-2015. Dotted and solid green contours enclose areas with significant values at the 95% and 99% level, respectively. The significance is determined using a Monte-Carlo approach.

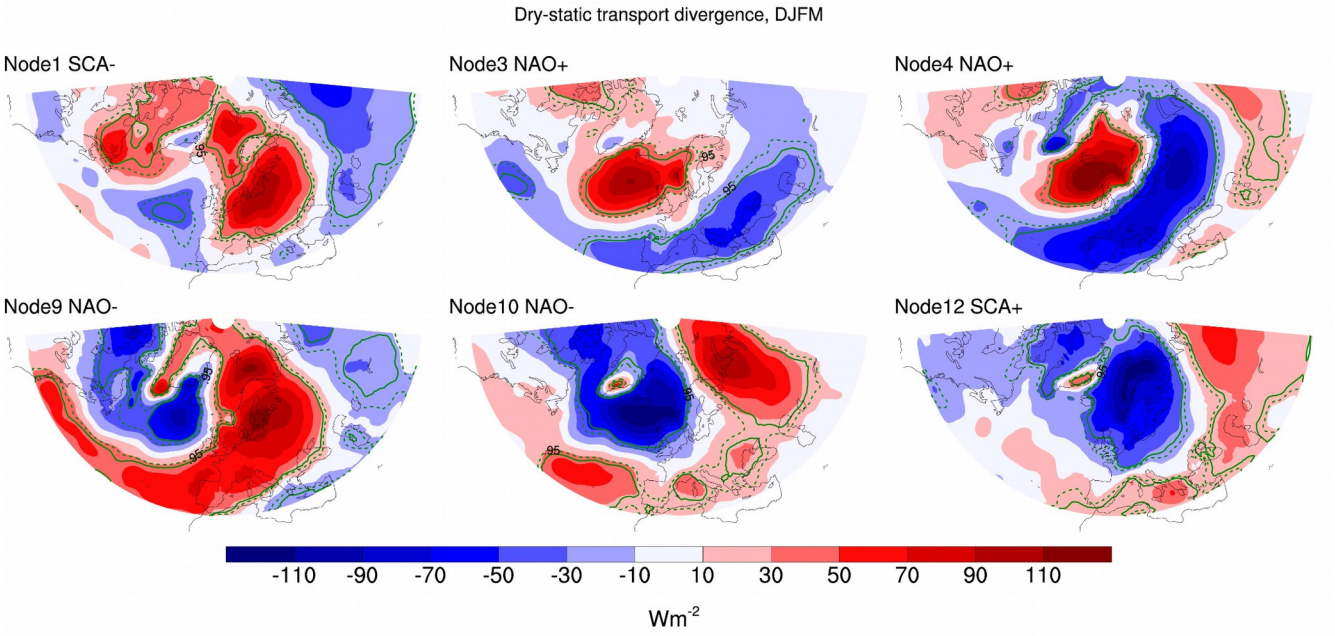

Figure 5. Same as Figure 4 but for the divergence of vertically-integrated dry static energy transport.

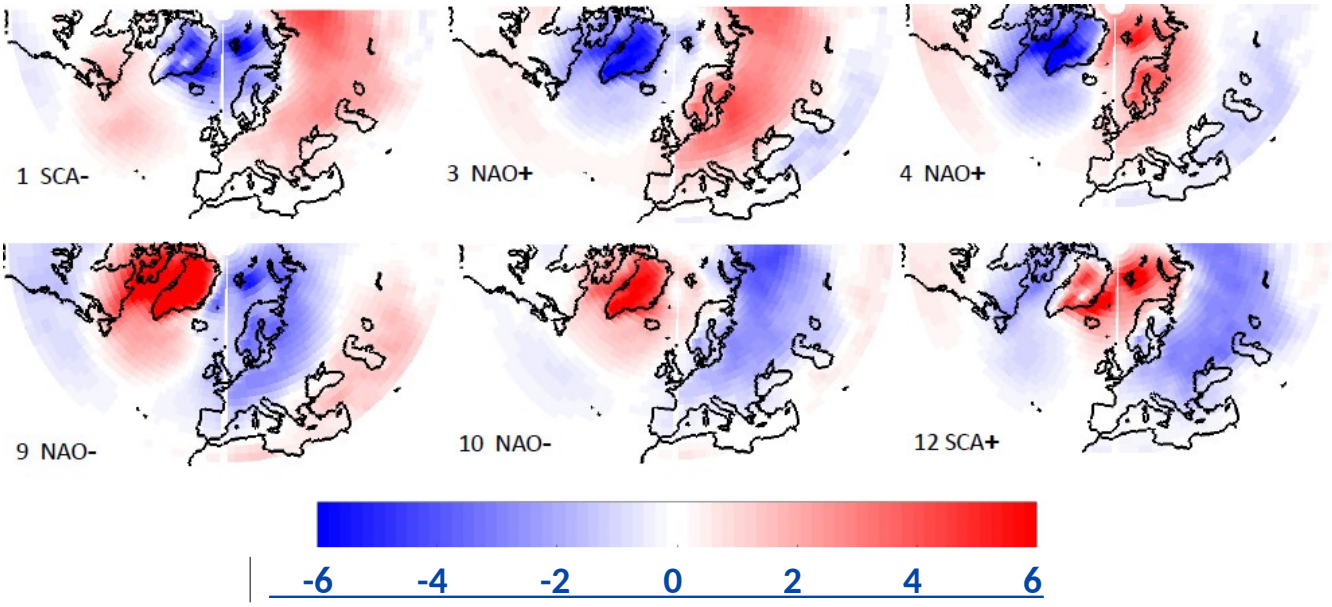

Figure 6. 2-m temperature anomalies (in °C) for winter (DJFM) in 1979-2015 projected on the same SOM nodes as in Figure 4.

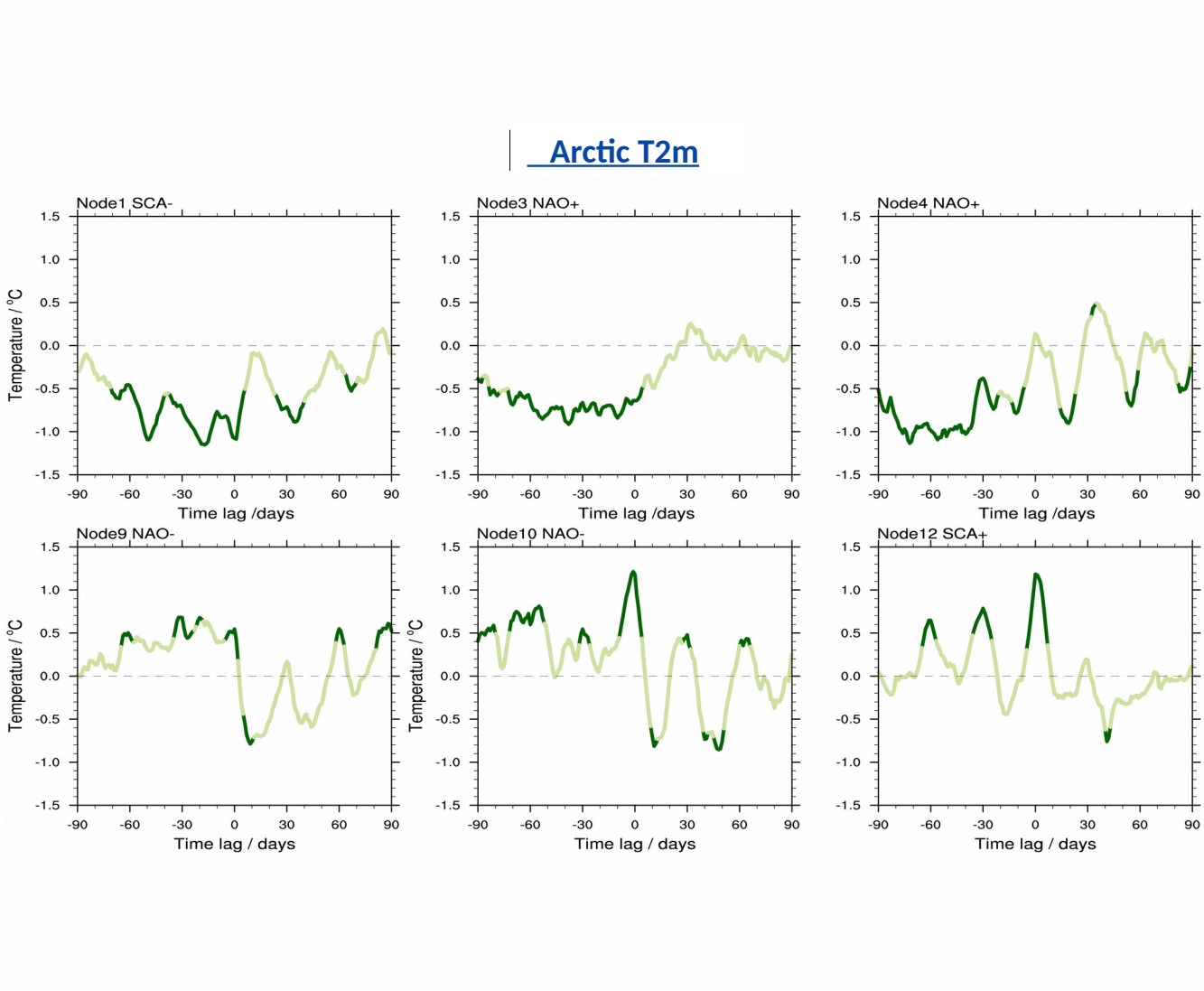

Figure 7. Composites of Arctic (north of 70°N) winter (DJFM) 2-m air temperature anomalies as a function of time lag with respect to the six most common large-scale circulation patterns identified by the SOM analysis. Dark lines indicate significance at the 95% confidence level. The significance is determined using a Monte-Carlo approach.

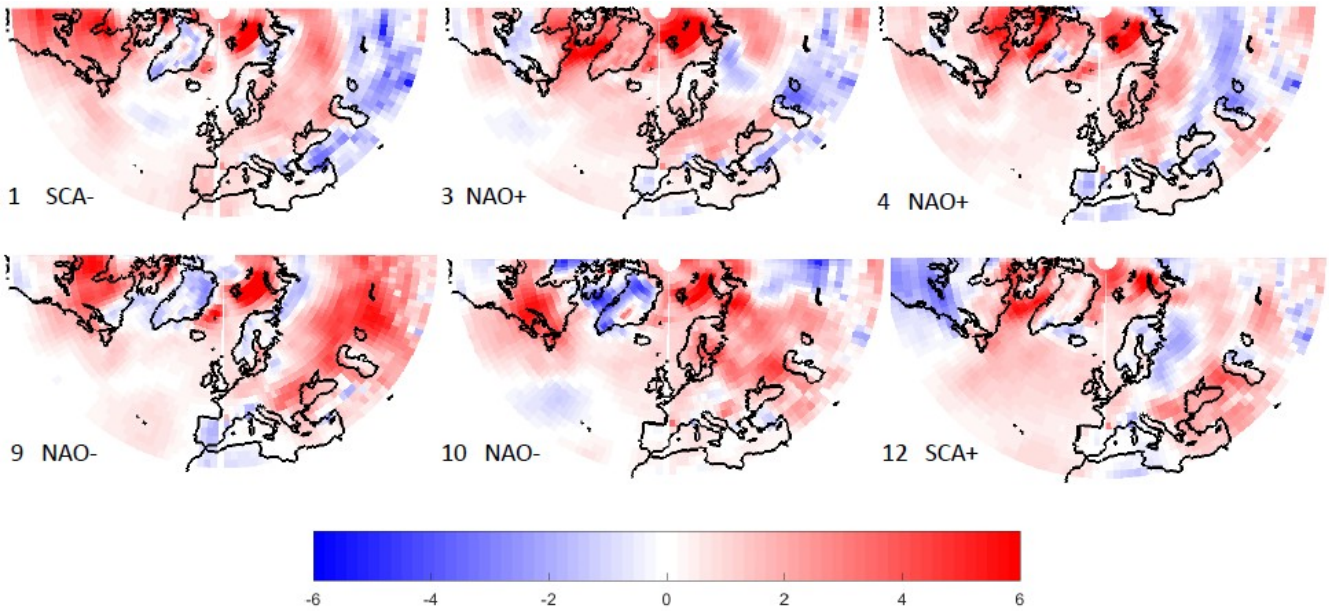

Figure 8. Difference in DJFM 2-m temperature anomalies, 1998-2015 minus 1979-1997, for the same SOM nodes as in Figure 5.

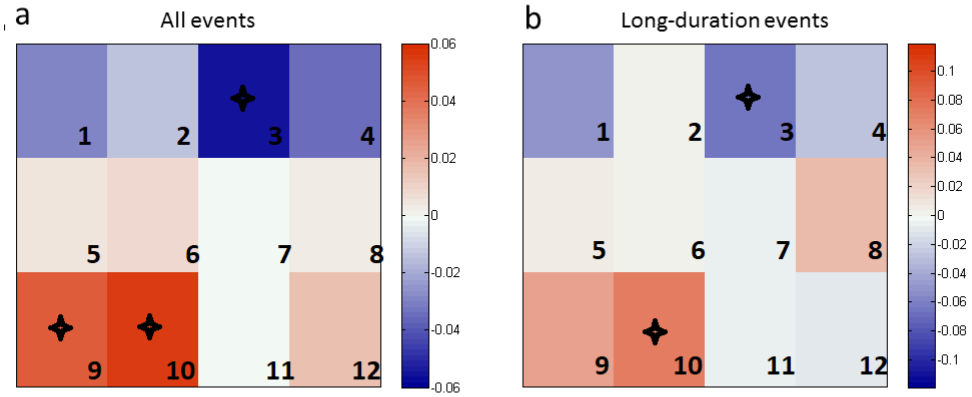

Figure 9. Changes in the relative frequency of occurrence of the winter circulation patterns identified by SOM analyses illustrated in Fig. 4 for (a) all events and (b) solely for cases when the atmosphere has resided in the same pattern ~~events that have lasted~~ for at least four consecutive days. The asterisks mark the SOM nodes with a statistically significant ($p < 0.05$) changes.

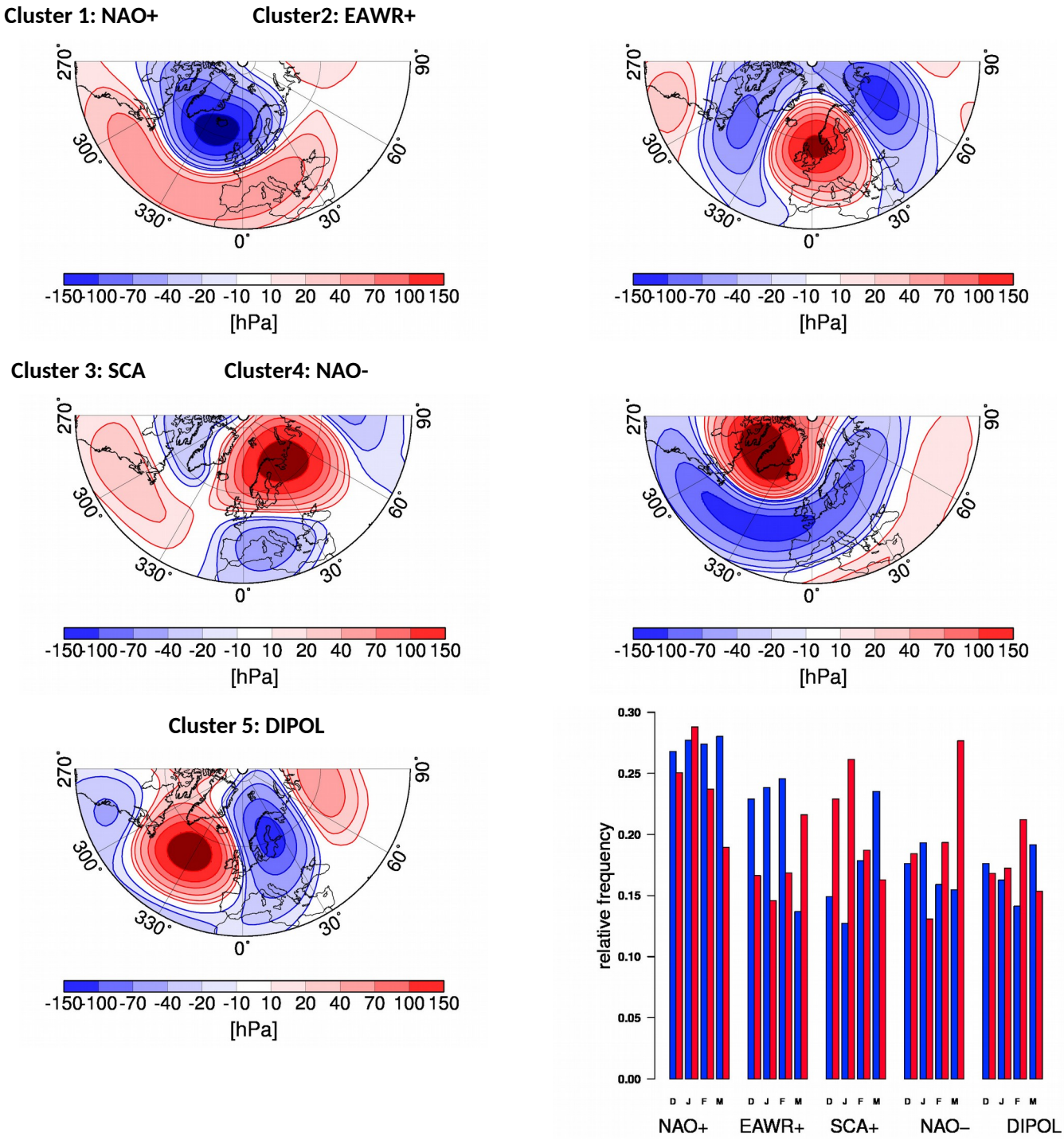

Figure 10. Geopotential anomalies at 500 hPa for the five most common large-scale patterns obtained by a cluster analysis using winter (DJFM) ERA-Interim data. Histogram shows the relative monthly

frequency of occurrence of each cluster, where blue and red bars are for the periods 1979-1997 and 1998-2015.

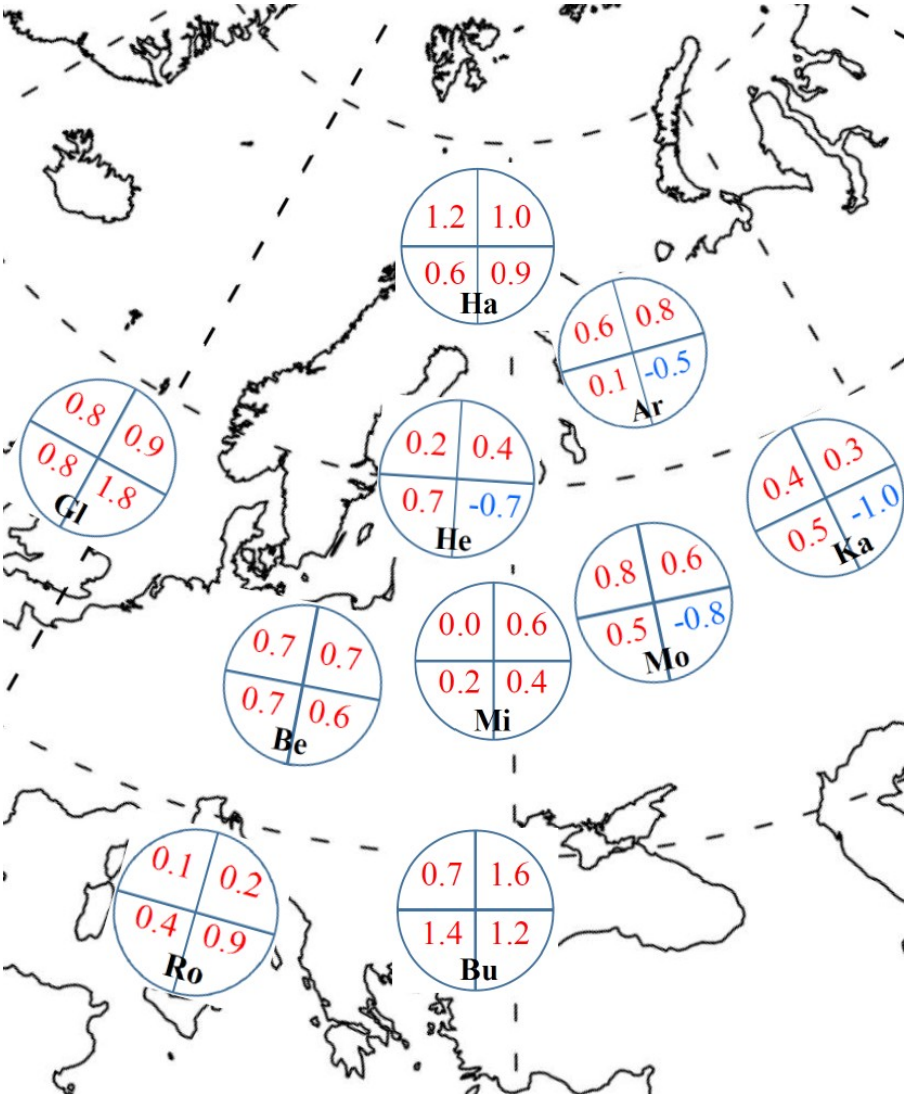

Figure 11. Differences in winter (DJFM) mean air temperature (°C) at 1 km height between the periods 1998-2015 and 1979-1997 in cases of airmass origins in the northwest, northeast, southeast, and southwest (noted in corresponding quadrants of circles) for Archangelsk (Ar), Berlin (Be), Bucharest (Bu), Glasgow (Gl), Hammerfest (Ha), Helsinki (He), Kazan (Ka), Minsk (Mi), Moscow (Mo), and Rome (Ro).

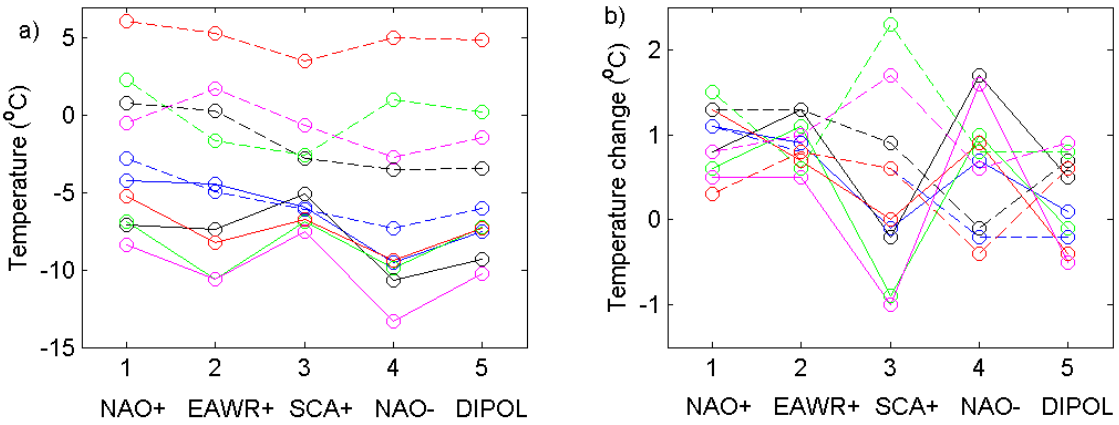

Figure 12. (a) Winter (DJFM) mean air temperature at 1 km height over the selected cities during 1979-2015 for the five circulation patterns identified on the basis of cluster analysis, and (b) the temperature difference between periods 1998-2015 and 1979-1997, for Helsinki (blue solid lines), Hammerfest (black solid lines), Kazan (green solid lines), Moscow (red solid lines), Archangelsk (magenta solid lines), Minsk (blue dashed lines), Berlin (black dashed lines), Bucharest (green dashed lines), Rome (red dashed lines), and Glasgow (magenta dashed lines).

Supplementary Material

Supplementary Table S1. Relative occurrence (in %) of the 12 SOM nodes during cold and warm events, lasting at least four days, in the five European regions marked in Figure 1: CE: Central Europe 45°N-55°N, 0°-20°E; SE: Southern Europe 35°N-45°N, 10°W-35°E; NE: Northern Europe 55°N-70°N, 5°E-25°E; WE: Western Europe 50°N-60°N, 10°W-5°E; EE: Eastern Europe 45°N-55°N, 20°E-40°E

SOM node	Cold WE	Cold NE	Cold EE	Cold CE	Cold SE	Warm WE	Warm NE	Warm EE	Warm CE	Warm SE
1	19	24	33	34	12	17	23	0	24	16
2	7	6	1	3	1	3	0	0	3	6
3	18	4	17	18	16	0	38	50	27	12
4	4	7	11	3	12	24	8	50	3	6
5	9	4	3	5	4	0	0	0	15	10
6	5	2	1	8	3	0	0	0	9	4
7	7	5	1	1	4	3	0	0	0	8
8	4	3	4	5	11	10	0	0	6	0
9	8	10	9	6	4	0	0	0	0	18
10	8	12	5	9	4	0	0	0	0	10
11	1	1	2	3	1	0	0	0	3	2
12	11	20	11	6	27	41	31	0	9	10

Supplementary Table S2. March mean temperature (°C) at 1 km height in Kazan, Moscow, and Archangelsk and the occurrence (in %) of five large-scale circulation patterns based on cluster analysis, in periods 1979-1997 (P1) and 1998-2015 (P2).

City	T(1km)		C1, NAO+		C2, EAWR		C3, SCA+		C4, NAO-		C5, DIPOL	
	P1	P2	P1	P2	P1	P2	P1	P2	P1	P2	P1	P2
Kazan	-4.4	-6.2	26	23	10	9	25	34	9	25	29	9
Moscow	-5.2	-6.0	28	20	5	10	35	27	11	27	20	17
Archangelsk	-9.4	-10.7	22	18	4	21	36	13	19	31	19	18

Supplementary Table S3. Changes in cloud variables from 1979-1997 to 1998-2015 for all air-mass origins

City	Cloud liquid water (kg m^{-2})		Cloud frozen water (kg m^{-2})		Total column water (kg m^{-2})		Total cloud cover (0-1)	
	All data	SE orig	All data	SE orig	All data	SE orig	All data	SE orig
Archangelsk	0.0041	0.0036	0.0009	0.0042	0.03	-0.22	0.01	0.03
Helsinki	0.0053	-0.0009	0.0003	0.0018	0.16	-0.09	0.01	0.07
Kazan	0.0053	0.0054	0.0029	0.0039	0.30	0.04	0.02	0.04
Moscow	0.0051	0.0050	0.0019	0.0045	0.29	0.13	0.01	0.07

Supplementary Figures

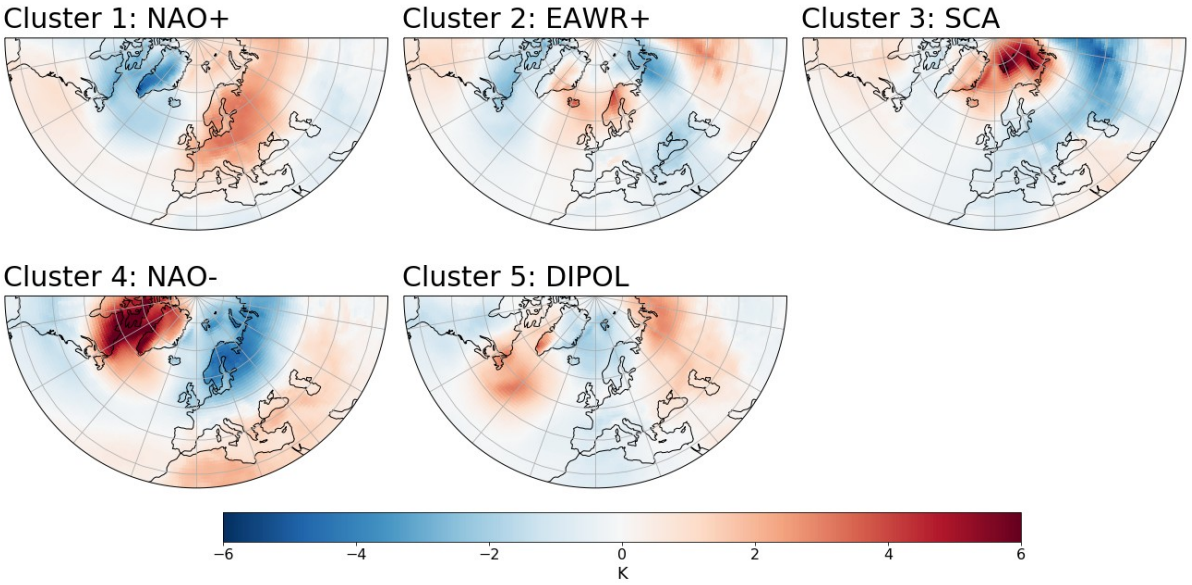

Supplementary Figure S1. As Figure 6 but based on the cluster analysis.

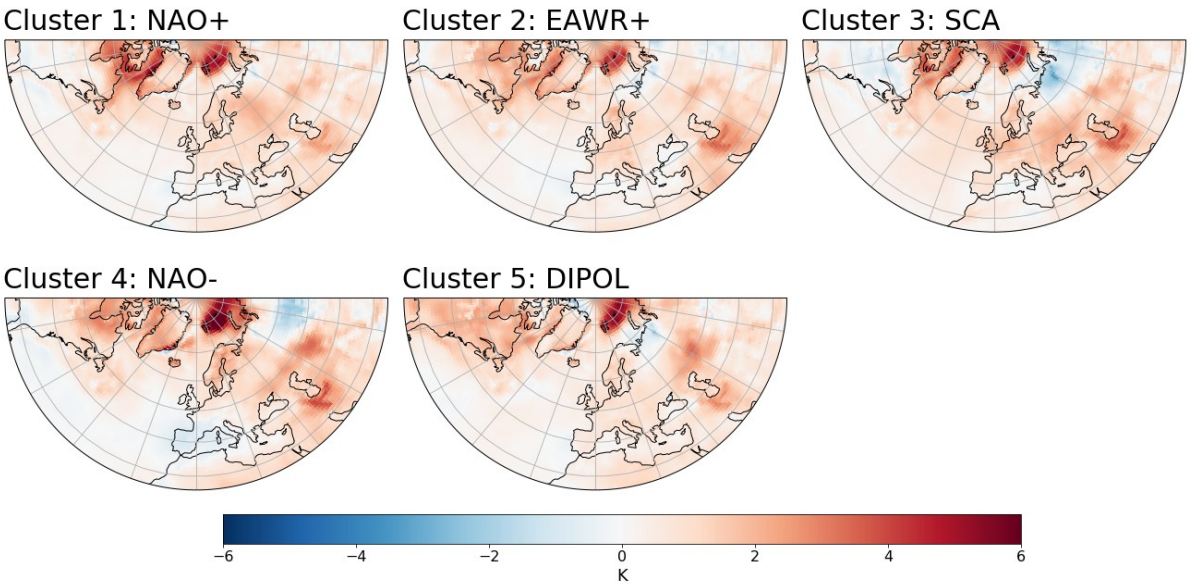

Supplementary Figure S2. As Figure 8 but based on the cluster analysis.

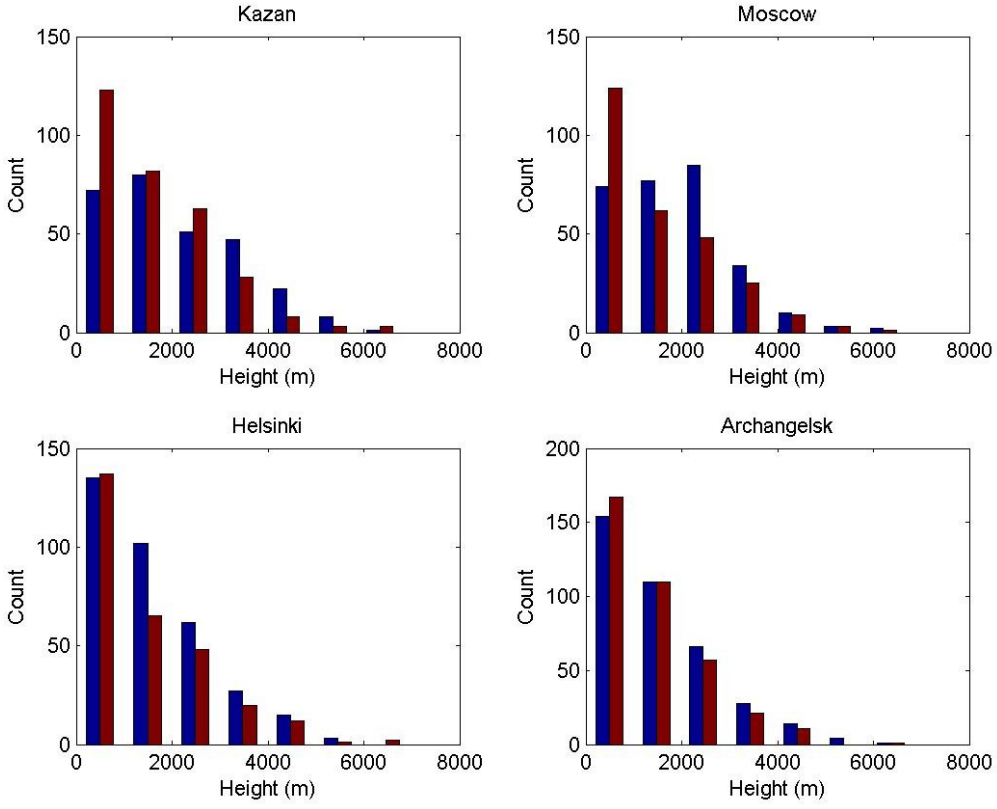

Supplementary Figure S3. Histograms of the start heights of the 5-day backward trajectories ending at Kazan, Moscow, Helsinki, and Archangelsk. The results for the period 1979-1997 are marked in blue and those for 1998-2015 in red.